IEEE Access
Multidisciplinary ⋮ Rapid Review ⋮ Open Access Journal

Received 6 April 2023, accepted 1 May 2023, date of publication 15 May 2023, date of current version 16 June 2023.

Digital Object Identifier 10.1109/ACCESS.2023.3276716

TOPICAL REVIEW

A Review of the Recent Applications of Aluminum Nitride-Based Piezoelectric Devices

SYED T. HAIDER[1,2], MUHAMMAD A. SHAH[1], DUCK-GYU LEE[1], AND SHIN HUR[1,2]
[1]Department of Nature Inspired Nano Convergence Systems, Korea Institute of Machinery and Materials, Daejeon 34103, Republic of Korea
[2]Nano Mechatronics, University of Science and Technology, Daejeon 34103, Republic of Korea

Corresponding author: Shin Hur (shur@kimm.re.kr)

This work was supported in part by the Human Plus Convergence Research and Development Program funded by the National Research Foundation of Korea and ICT and Future Planning under Grant NB1940; in part by the Material Parts Technology Development Project (Development of High Resolution Inkjet Head for Flat Display) funded by the Ministry of Trade, Industry, and Energy (MOTIE), South Korea, under Grant MT4130; and in part by the Korea Institute of Machinery and Materials (KIMM) through the Research Program under Grant NK244E.

ABSTRACT Piezoelectric materials have attracted considerable attention over the last two decades because many technologies utilize their core properties of piezoelectric materials. Previous applications consisted of bulk structures; however, a shift towards better performance and a more simplified and compatible fabrication method are required. Aluminum nitride (AlN) is a material that fits these criteria; it has a non-centrosymmetric crystal structure with a polarized c-axis and exhibits piezoelectric properties. Furthermore, it has an added benefit as the fabrication process of AIN is compatible with complementary metal–oxide semiconductor technology. This has led to a rapid increase in the adoption and interest in AlN-based devices. In this review, the crystal structure of AlN and its piezoelectric properties are compared with those of aluminum scandium nitride. Subsequently, functional devices such as consumer-based devices, telecommunication-based devices, industrial-related applications, and medical applications are presented. Finally, a summary and discussion of the future AlN research are presented.

INDEX TERMS Aluminum nitride, scandium, piezoelectric, MEMS, device.

I. INTRODUCTION

Mutual conversion of mechanical and electrical energy can be achieved using a piezoelectric element. Piezoelectric materials have found a variety of applications in various fields, including as filters in communication systems [1], [2], resonators [3], ultrasonic medical devices [4], piezoelectric motors [5], speakers [6], [7], and sensors [1], [6], as shown in Fig. 1. Although the bulk of the existing market share of piezoelectric sensors remains high, challenges such as reduced power consumption, miniaturization, and more environmentally friendly fabrication processes still need to be solved as the demand for high-performance devices increases. Materials such as Lead Zirconate Titanate (PZT) [8], Zinc Oxide (ZnO) [9], and Gallium Nitride (GaN) [10] have been studied extensively. However, it is evident from the literature that tradeoffs exist between material selection, performance, and fabrication processes.

Aluminum nitride (AlN) has recently attracted considerable attention because of its ability to exhibit a high phase velocity [11], [12], high stiffness coefficients [11], [12], [13], and a relatively low dielectric constant [13], [14]. Moreover, the compatibility of complementary metal–oxide semiconductor (CMOS) fabrication to form monolithic devices has allowed for easy fabrication processes [14]. In addition, compared with materials such as PZT, its piezoelectric properties are weak; therefore, recent AlN developments include enhancement its piezoelectric properties, such as through doping with various metals, such as Sc [15], [18], V [16], Ti [17], Ta [20], Mg [20], and others [20]. Among these metals, Sc stands out, and up to 40% of doped cases of Sc-doped AlN have been studied [18], [19]; the piezoelectric properties have been found to increase by up to five times for the case of a 40% Sc-doping ratio. In addition, other research

The associate editor coordinating the review of this manuscript and approving it for publication was Gustavo Callico.

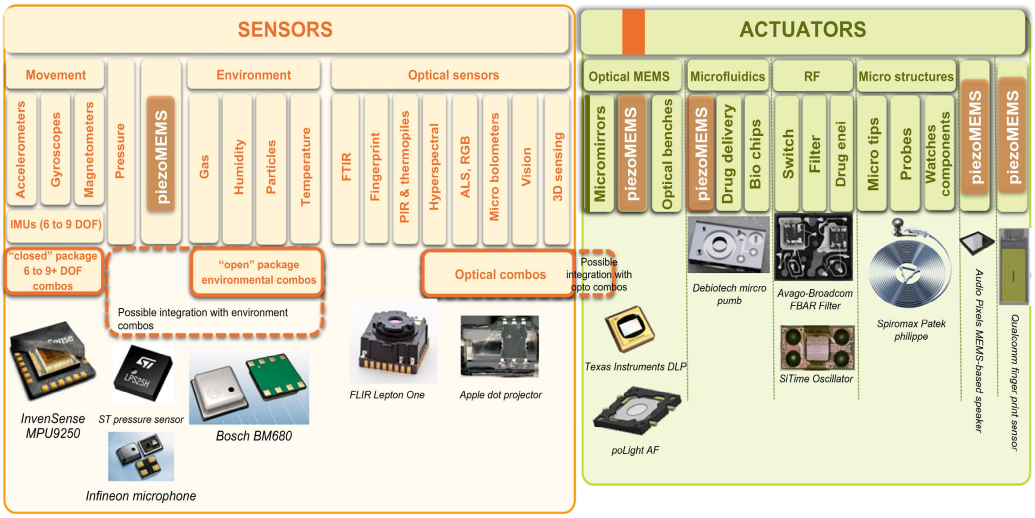

FIGURE 1. Chart explaining various applications of piezo materials [25].

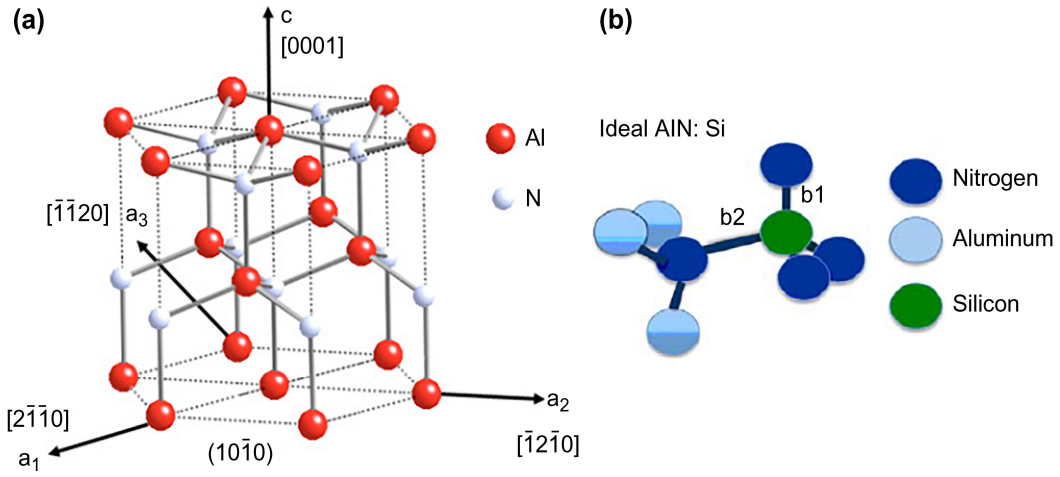

FIGURE 2. (a) AlN crystal structure [31], (b) Bond conureuration showing the position of B1 and B2 bonds [32].

areas related to integrated photonics have shown excellent performance in terms of optical [21], [22] and pyroelectric properties [23], [24].

This review summarizes the recent research on the use of AlN in commercial-scale devices over the past decade. Section II briefly discusses the AlN structure and compares the piezoelectric properties of AlN and aluminum scandium nitride (AlScN). Section III presents recent developments in AlN for consumer applications, including piezoelectric micromachined ultrasonic transducers (PMUT) devices, energy harvesters, speakers, and microphones. Developments in telecommunications are presented in Section IV, followed by industrial developments in Section IV.

Next, we present recent research on AlN in Blood pressure monitoring as part of medical applications, and finally, an overview of its possibilities

II. AlN CRYSTAL STRUCTURE

AlN belongs to the III–V family because it forms a hexagonally packed wurtzite structure, as shown in Fig. 2(a). The lattice parameters for the a- and c-axes were approximately 3.110 and 4.978 Å, respectively. Fig. 2(b) shows the crystalline structure of AlN. The tetrahedral structure consists of each Al atom bonded to four N atoms, three of which are B1 bonds and one is a B2 bond. The maximum piezoelectric response d_{33} was measured to be approximately 5.5 pC/N and was obtained in the longitudinal direction [26], [27], [28], [29], [30]. In addition, a high stiffness C_{33} was measured at $3.67e^{11}$ N/m^2. The intrinsic Q factor of AlN and its compatibility with CMOS fabrication processes are important design features of bulk acoustic wave (BAW) resonators and filters.

The most critical design aspect of a piezoelectric device is its crystal quality, which is affected by the thickness of the piezoelectric layer. Studies have revealed that, with an increase in thickness, the d_{33} property increases, but the dielectric loss decreases. However, as the thickness increases to 1 μm, any further change in the thickness has minimal effect on the crystal quality of the AlN film [29], [30].

Barth et al. [33] used reactive magnetron sputtering to form AlN films using Al and Sc as targets. By varying the target

power ratio, the Al-to-Sc ratio can be easily changed over a wide range, from pure AlN to $Al_{(1-x)}Sc_{(x)}N$, where x = 0.4. An increase in the value of x from 0 to 0.40 increases the d33 coefficient and decreases the Young's modulus. Recent studies have focused on Sc-doped AlN. Table 1 compares the piezoelectric properties of AlN, 20% Sc-doped AlN, and 40% Sc-doped AlN.

TABLE 1. Comparison of piezoelectric properties of AlN, AlSc(0.2)N, AlSc(0.4)N, taken from various resources [33], [34], [35], [36], [37].

Properties	AlN	AlSc(0.2)N	AlSc(0.4)N
Piezoelectric Constant (C/m^2)	e_{31} = -0.58 e_{33} = 1.55	E_{31}=-0.62 E_{33}=1.67	E_{33} = 3.19
Piezoelectric Coefficient (pC/N)	D_{33} = 5.5 D_{31} = -2.65	D_{33}=20	D_{33} = 20 - 25
Electromechanical coupling coefficient k^2	>1%	>2%	3.8 % to 4.5 %
Elastic Modulus (GPa)	338	240	193
Hardness (GPa)	23	20	13
Elastic Constant C_{11} GPa	345	320	298
Elastic Constant C_{12} GPa	125	127	143
Elastic Constant C_{13} GPa	125	126	132
Density kgm^3	3453	3560	3680

III. APPLICATIONS

A. CONSUMER APPLICATIONS

Currently, mass-produced consumer devices are not only confined to very large-scale integrated circuit (VLSI) devices, but also have an integrated piezoelectric device that works in a variety of applications, such as fingerprint sensors [38], [39], microphones [40], and speakers [41]. In addition, devices that require a large voltage bias, such as capacitive micromachined ultrasonic transducers (CMUT), are not beneficial. However, PMUT devices can be actuated at a low-voltage bias and generate electric signals when acted upon by an external force [42], [43]. Further enhancements, such as integration with complex but small-footprint CMOS circuitry, have allowed an increasing number of devices to be built on a single platform. This paper presents a review of recent developments in AlN-based piezoelectric devices for consumer electronics, including PMUT devices, microphones, speakers, and energy harvesters. A brief description of recent progress, along with a comparison of recently developed devices, is provided in each section.

1) AlN-BASED PMUT

A PMUT device utilizes piezoelectric phenomena for electroacoustic conversion, ultrasonic transmission, and reception over a wide range of frequencies. Depending on the frequency range, PMUT devices have been used extensively for fingerprint sensing [38], [39], medical imaging applications [40], [42], and vein identification [43], [44], [45], [46]. Studies on CMUT have also been conducted [46]. However, limitations such as inaccuracy owing to oily or wet hands, low ultrasound intensity, high-voltage biasing, power consumption, and pulling effects are considered disadvantages in practical applications. Hence, interest in PMUT-based devices has recently increased [47], [48].

A fingerprint device captures an image of a human fingerprint by utilizing various phenomena, such as optical sensing [49], [50], capacitive sensing [51], and pressure sensing [51]. Recently, ultrasound fingerprint sensors have attracted considerable interest owing to their design innovations and because they are unaffected by contamination and moisture in the human hand. The PMUT sensor transmits ultrasound waves between the fingerprint frames and valleys, and based on the time-of-flight change, an image can be developed for a human fingerprint [52], [53], [54].

Munoz et al. [55] presented a circular PMUT comprising multiple electrodes for differential transduction. The design comprises an AlN layer with Al electrodes and different elastic layers. The PMUT device with Si3N4 showed an improved output pressure compared with the design using SiO2 and a-Si as elastic layers. The PMUT device developed by Ledesma et al. [56] uses a square block of an AlN layer with both Al electrodes and a Si3N4 layer as the passive material, as shown in Fig. 3. The use of multiple top electrodes for differential transduction with a common bottom electrode resulted in a higher device sensitivity and coupling efficiency than those achieved in the literature [57]. Compared to a circular PMUT, a square PMUT has a better output performance as the fill factor and output pressure are larger. This device was then expanded to a 6 × 6 PMUT array so that its performance as both an actuator and sensor could be observed. Similarly, a 6 × 6 array is designed [58]. The PMUT array was fabricated at Silterra Malaysia Sdn using a microelectromechanical system (MEMS)–on–CMOS process [59]. In their design, both square and circular PMUT arrays were presented with fill factors of 50% and 65%, respectively. However, as described by the authors, both devices yielded similar results. This research was further enhanced by developing guidelines to optimize the PMUT device, and the results were compared with those of previous studies [60]. The guidelines consist of performing a finite element method (FEM) analysis by varying the thicknesses of the passive layer, AlN layer, and inner electrode sides. Based on the design parameters, a figure of merit (FoM) was developed using the equation $\text{FoM} = d_0 x f^2 x V r^2$, where d_0 is the membrane displacement, f is the resonant frequency, and V_r is the output voltage between electrodes.

A higher acoustic output was obtained with a thinner PMUT with 0.6 μm AlN thickness and 1 μm Si_3N_4 thickness. The 110 × 56 PMUT array designed by Jiang et al. [61] is composed of rectangular PMUTs with a fill factor of 51.7%. This allowed them to achieve a lateral resolution of 75 μm and an axial resolution of 150-micron for a 4.6 × 3.2 mm image. An application-specific integrated circuit (ASIC) interface was designed using a standard 180 nm CMOS process. The PMUT array size was similar to that used in many

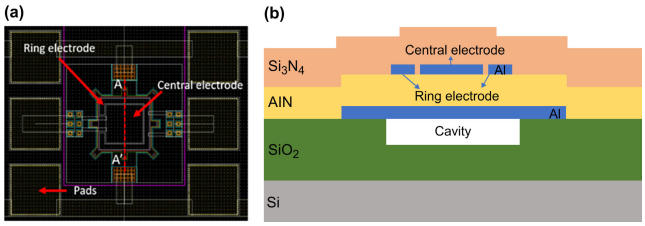

FIGURE 3. View of a PMUT design (a) PMUT, (b) Cross-sectional area with layer arrangements taken from [60].

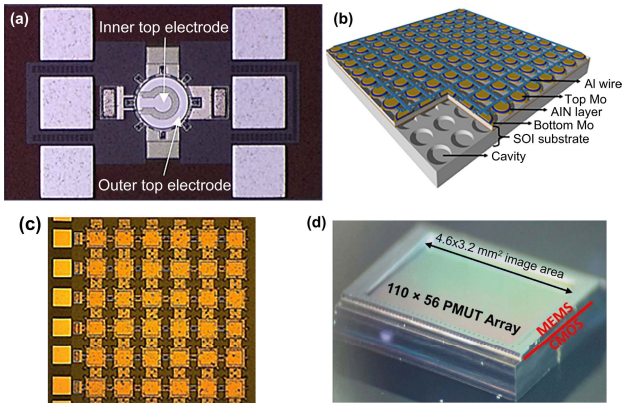

FIGURE 4. Illustrations of various PMUT devices, (a) PMUT based on a dual-electrode [56], (b) 3D diagram of AlN PMUT array [63], (c) 6 × 6 PMUT array based on a square-shaped PMUT design [58], (d) 110 × 56 PMUT on a CMOS structure [62].

smartphones today, and the element pitch (591 × 438 DPI) was comparable to the resolution of commercial capacitive fingerprint sensors. Additional experiments included imaging of the epidermal and subepidermal layers. The results were compared with optical fingerprint images, and good agreement was observed [62]. A comparison of the different PMUT designs and their important features is presented in Table 2.

2) AlN-BASED MICROPHONES

There is a wealth of information on MEMS-based microphones, focusing much on microphones for consumer audio applications. The specifications of an aeroacoustic measurement microphone differ significantly from those of an audio microphone. In the former application area, the criteria for bandwidth (10–15 kHz) and maximum pressure (commonly 120 dB) are not as crucial as those for the lowest detectable pressure (approximately 30 dB) in air. Depending on the measurement, the maximum pressure and bandwidth requirements for the microphones used for aeroacoustic measurements may occasionally reach or exceed 160 dB and 100 kHz, respectively. By contrast, the noise floor is less important for audio microphones. In this portion of our review paper, we focused on AlN-based piezoelectric MEMS microphones designed for acoustic applications and consumer audio applications.

Low dielectric loss, high intrinsic signal-to-noise ratio, high rigidity, and a high material figure of merit for sensitivity are attractive properties of aluminum nitride (AlN) [68], [69]. The low dielectric loss of AlN is a crucial advantage over PZT and ZnO for fuselage array applications, because it results in an improved low-frequency microphone response. Consequently, AlN has been used in aeroacoustic applications [70]. Aeroacousticians employ an AlN-based micromachined microphone for aircraft fuselage arrays to pinpoint aircraft noise sources and evaluate the efficacy of noise-reduction solutions. An ideal design was created and characterized by Avago Technologies. The manufactured instrument has a sensitivity of 39 V/Pa and a maximum detectable pressure of 172 dB at a 3% distortion limit. The instrument responded flatly between 69 kHz and 20 kHz. Littrell [71] proposed a double-layered AlN/Mo cantilever-based piezoelectric microphone as part of his doctoral dissertation at the University of Michigan. The goal of this project was to demonstrate a piezoelectric microphone with reduced noise levels. Two different types of device were created for this project. The first suggested device is a grid of 20 cantilevers with 0.5 μm thick AlN layers that serve as sensing elements. However, owing to the significant dielectric loss and subpar film quality, the test results revealed a noise floor higher than the anticipated value of 58 dB. The stress in the cantilever construction also caused a decrease in vent resistance. The first device has been modified with thicker AlN (thickness:1 μm) to achieve improved quality of the AlN film. AlN and Mo were individually patterned owing to changes in the fabrication process. The number of cantilevers was reduced from four to two to close the space surrounding them, which increased the vent resistance. The fabricated device resonated at 18 kHz and exhibited a sensitivity of 1.82 mV/Pa and low noise floor level. In [72], the authors demonstrated an AlN-based MEMS directional microphone (shown in Fig. 5) in the d_{33} mode. The ability of AlN to reduce thermomechanical noise and the d33 mode were used to obtain a higher output response. Consequently, the SNR and noise floor of this combination were higher and lower, respectively, than those of the other combinations. Another MEMS microphone with an enhanced SNR using AlN and d_{33} modes was presented in [73]. In reference [74], the authors presented an AlN-based circular membrane microphone with reduced stress by introducing segmented electrodes. Table 3 provides an overview of the major sensor parameters and the chronological contributions of researchers. This summary will assist researchers in assessing the actual performance of any given AlN-based piezoelectric MEMS microphone device.

3) AIN-BASED SPEAKERS

The last decade has seen rapid advancements in consumer electronics, and a rapidly changing market has increased demand for small, compact, and low-power-consumption devices that outperform all previous devices. Speakers are a core component of mobile devices, laptops, wireless earbuds, and human–machine interfaces. Currently, speakers in commonly available consumer devices are dominated by bulky moving-coil-based designs. Although this is a mature technology, batch fabrication is challenging because voice

TABLE 2. Comparison of different PMUT-based devices.

Author	Device	Material	Size	Resonant Frequency.	Output pressure	Comments
Mufioz et al. [55]	Circular PMUT	AlN	80 µm x 1.3 µm	5.64 MHz	8 Pa – 50 Pa	Q=222. The device was tested with passive layers of SiO2, a-Si, Si3N4
Ledesma et al. [56]	Squared PMUT	AlN	80 µm x 1.3 µm	5.9 MHz	388 Pa in H2O and 360 Pa in FC-70 fluid	MEMS–on–CMOS process
Ledesma et al. [58]	6x6 Array	AlN	80 µm x 1.3 µm	NA	670 Pa	SR = V/MPA = 5.9
Horsley et al. [62]	110 × 56 Array	AlN	30 µm × 43 µm x 1 µm	16 MHz	15 KPa 0.6 µV Pa^{-1}	Claimed to be the first to image epidermis and sub-surface layer fingerprints
Lu et al. [63]	44 x 39 Array	AlN	25 µm × 1 µm	16 MHz	1000 Pa in air and 10,000 Pa in water	Arrays fabricated on a double-side polishing SOI wafer with customized cavities
Ledesma et al. [67]	Square	AlN with 9.5% Sc-doped	80 µm x 1.2 µm	2.48 MHz	1.77 kPa	Piezoelectric coefficient (kt^2) in air and liquid is 2.76 % and 1.12 %

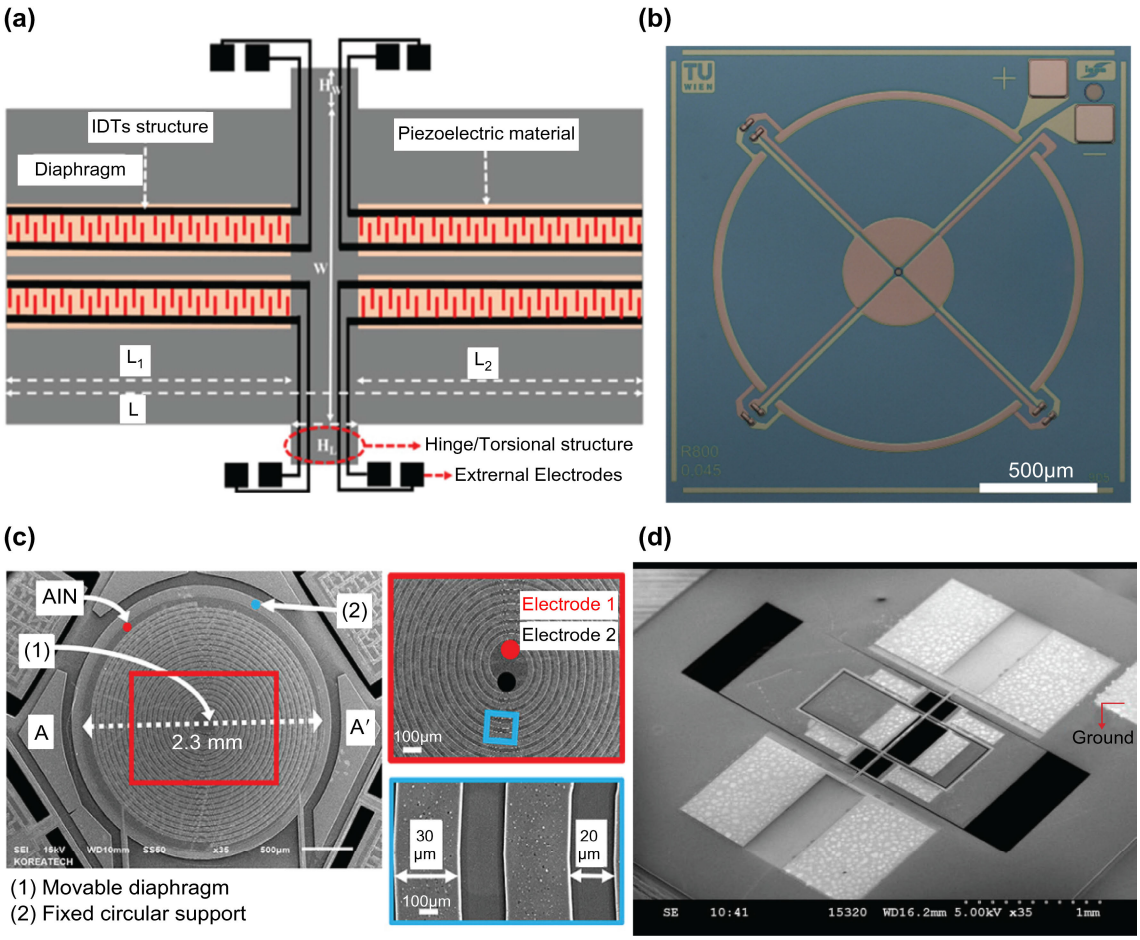

FIGURE 5. Illustration of various MEMS microphones, (a) Directional microphone based on interdigitated electrodes, referenced from [72], (b) microphone based on segmented electrodes, taken from [74], (c) interdigitated electrodes-based microphone taken from [73], (d) directional microphone taken from [77].

coils and permanent magnets must be assembled. By contrast, MEMS-based speakers, or microspeakers, have attracted more attention owing to factors such as low power consumption, small device footprint, batch fabrication, and compatible integration with electronic circuits [81].

PZT-based thin-film speakers are the most commonly available type of material used in fabrication processes; however, their nonlinear actuation is due to their ferroelectric properties and the lack of an environmentally friendly fabrication process [82]. ZnO [83] and AlN [84] are commonly used MEMS piezoelectric thin films. In addition, mature fabrication techniques allow thin films to be deposited by reactive magnetron sputtering methods [83], [84], [85]. However, from a commercial perspective, only a handful of AlN MEMS speakers are currently available on the market [86].

TABLE 3. Performance comparison of AlN-based piezoelectric MEMS microphones.

Author	Membrane		Sensitivity	Bandwidth
	Size	Thickness		
Fazzio et al. [75]	0.7mma	0.3	NA	1 – 6 KHz
Cho et al. [76]	N/A	0.5	N/A	100 Hz – 15 kHz
Williams et al. [70]	0.82 mm[a]	2.14	39 mV/Pa	69 Hz – 20 KHz
Littrell et al. [71]	0.62 mm^2 area	1[b]	1.82 mV/Pa	50 Hz – 8 KHz
Zhang et al. [77]	1 mm[d]	0.5	19 mV/Pa	100 Hz – 15 kHz
Fernandez et al. [78]	1.6 mm[a]	0.2	0.68 mV/Pa	11.2[e]
Rahaman et al. [72]	0.81 mm[e]	0.5	5.43 mV/Pa	20 Hz – 20 kHz
Rahaman et al. [73]	2.3 mm[a]	0.5	4.49 mV/Pa	2 kHz – 10 kHz
Ullmann et al. [74]	1 mm*	0.36	0.46 mV/Pa	10 Hz – 10 kHz
Kumar et al. [79]	1.7 mm[c]	0.3	N/A	12 Hz – 22 kHz

[a]Diameter of membrane.
[b]Stacked AlN.
[c]Side of square membrane.
[d]Length of wing.
[e]Resonance frequency.
N/A: Not available

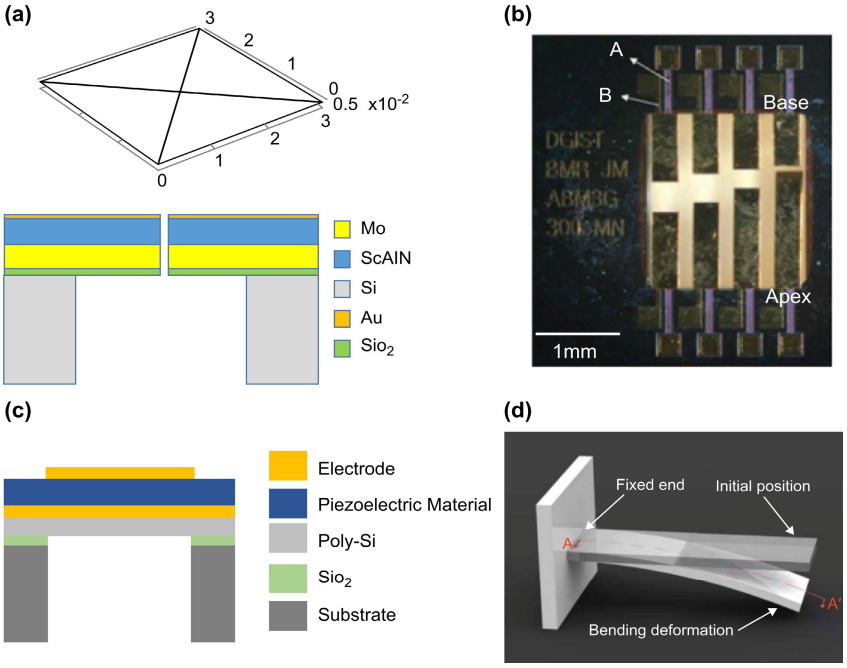

FIGURE 6. Illustration of various MEMS speakers. (a) Schematic of the MEMS ScAlN speaker with actuators separated by small gap [87], (b) optical image of the fabricated membrane with cantilevers [89], (c) cross-sectional view of the MEMS speaker designed with various selection of materials for electrodes and piezoelectric layers [88], and (d) schematic of a cantilever beam with bending under the applied electric field [90].

TABLE 4. AlN-based piezoelectric MEMS speakers.

Author	Material	Size	SPL (dB)	Power	Comments
Fawzy et al. [87]	$AlSc_{0.09}N$	1 µm	Up to 50 dB	20 V	Use of four actuators separated by a thin gap
Hossam et al. [88]	AlN	2 µm	NA	20 V	Comparison between various materials and electro de configuration
Jang et al. [89]	AlN	0.5 µm	95 dB	3.5 Vpp	Piezoelectric artificial basilar membrane
Liu et al. [90]	AlN	0.5 µm	101 dB	8 Vrms	Sensitivity 105–107 dB/mW, 10- times less power consumption

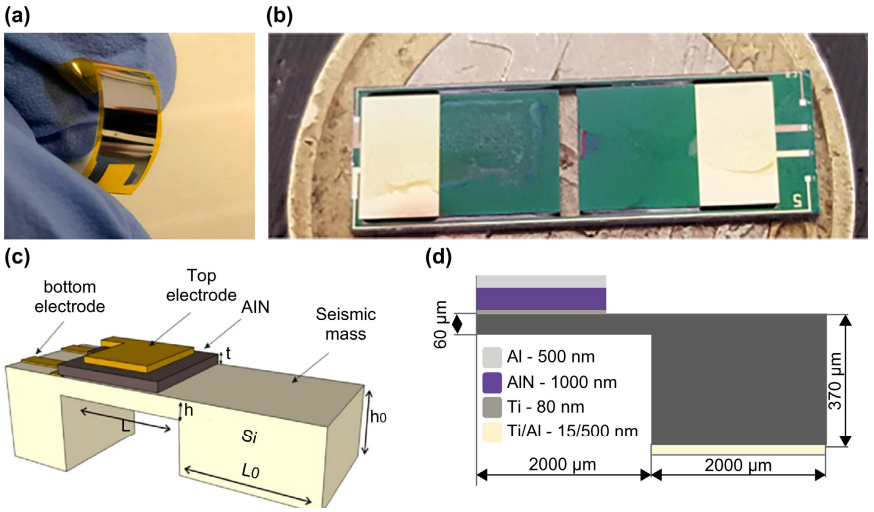

FIGURE 7. Illustration of various MEMS energy harvesters: (a) SEM image illustrating the cross-section view of the Piezo Harvester [102], (b) fabricated AlN-based MEMS energy harvester with a two-cantilever device [99], (c) device concept of the AlN harvester with seismic mass [98], and (d) layer composition and their dimensions of piezoelectric energy harvesters [103].

Fawzy et al. [87] developed a 9% Sc-doped AlN-based MEMS speaker and compared its piezoelectric coefficient to that of AlN. The design consists of four triangular actuators arranged in a stacked position. The actuators were separated from each other by small gaps. The thickness of each element was optimized using an analytical model. Additionally, the performance was affected by the gap between the actuators, and this function was sound pressure level (SPL). From the analysis, it was observed that as the distance became greater than 10 μm, the SPL magnitude decreased significantly. In addition, the deflections of AlScN and AlN were compared and it was observed that the deflection was higher for AlScN. In another study [88], the design parameters were varied to measure the membrane deflection and SPL output of the speaker. The performances of the membraneless and clamped designs were compared using different material arrangements and resonant frequencies. The best model was proposed based on this design. In terms of innovation, a novel artificial basilar membrane using a MEMS-based piezoelectric cantilever array was proposed [89]. The design parameters of the array considered the frequency selectivity and sensitivity to the incoming sound pressure, and AlN was used as the active piezoelectric layer sandwiched between the two electrodes.

Sensitivity is a key performance parameter when designing speakers because power consumption is a key factor when considering consumer-based applications such as electronics, medical devices, and Internet of Things (IoT)-based platforms. The SPL output is also related to the power consumption; a higher level of sensitivity results in lower power consumption. Liu et al. [90] developed an analytical model to optimize the sensitivity and SPL output of speakers. The key parameter of focus was the layer thickness ratio. The analytical expression consists of equations involving the piezoelectric model, tensile deformation, bending deformation, and derived displacement. For these expressions, the input ratio of the piezoelectric layer thickness to the support layer thickness was used, and an optimized model was created based on the response obtained.

4) AlN-BASED ENERGY HARVESTERS

Devices that promise a self-powered energy system and are employed indoors and outdoors can be utilized in various applications, such as remote and harsh environments, and embedded inside the human body, as in the case of pacemakers [91], [92], [93], [94].

Energy harvesting has recently attracted considerable attention from the research community as a key technology in applications where changing batteries is not practical, such as autonomous wireless sensor networks (WSN), IoT, and e-health. Among the available ambient energy sources suitable for energy-harvesting applications, ambient vibrations can provide a high energy density per unit device and operate in implanted or embedded systems [93], [94].

Several approaches have been developed for piezoelectric micro-and nanogenerators to harvest energy from random and tiny human body motions: one is through the use of nanostructured materials, and the other is through thin films [94], [95], [96].

Studies have been conducted to investigate the properties of AlN energy harvesters operating over a range of frequencies. Sharma et al. [97] developed an AlN on an SOI wafer and generated a total of 54 nW at a low level of acceleration of 24 mg at an operating frequency of 114 Hz. Dow et al. [98] fabricated an energy harvester based on two different design architectures and obtained output powers of 10 and 34.78 μW at resonant frequencies of 186 and 572 Hz, respectively.

Jackson et al. [99] demonstrated a novel technique using an AlN-based device to self-generate power for an implantable

leadless pacemaker that utilized heart vibrations and maintained a small footprint within the pacemaker capsule. At a low resonance frequency of 20–30 Hz and a small 'g' vibration of 1–1.5, an average power of 1.49 and 2.81 μW is obtained.

One technique for developing AlN films is sputtering [100], [101]. This technique is a promising approach for developing energy harvesting applications because AlN is a low-temperature preparation material with unique physical properties and is a highly thermally stable material with a melting point of approximately 2100 °C, with a piezoelectric effect study up to temperatures of approximately 1150 °C [101]. Additionally, an AlN-based piezo-cantilever beam was built on a silicon-proof mass. The piezoelectric thin film possessed a highly c-axis-oriented crystallite with a homogenous polarity distribution. The film was deposited using pulsed DC magnetron sputtering. During the process, parameters such as the vacuum degree, gas flow ratio of N2 and Ar, sputtering power, substrate temperature, presputtering time, and seed layer were systematically optimized and analyzed. The final AlN film was kept at 1μm to generate a total power of 55–56 μW at a resonance frequency of 210 Hz. Algeiri et al. [102] synthesized a flexible and biocompatible energy harvester using an AlN thin film sputtered onto a thin polymer substrate. The piezoelectric coefficient was found to be 4.93 $\pm$ 0.09 pm/V, optimal generated power was found to be 1.57 μW.

Frach et al. [100] used reactive-pulsed magnetron sputtering with a double-ring magnetron DRM 400 to develop AlScN films. Pure Al and Sc-targets were used to deposit AlN or $Al_xSc_{1-X}N$, respectively, with Sc concentrations up to 55%; based on the designs, an RMS power of 70 μW for AlN and 350 μW for AlSc(0.4)N were obtained and as the thickness was increased from 10 um to 50 μm the output power saw an increase to 140 uW. Recent studies have included other methods to develop a simpler fabrication process using multilayer ion beam-assisted deposition [103]. This method demonstrated a d_{33} coefficient of (7.33 $\pm$ 0.08) pCN^{-1} and an output power of 0.25 μW.

B. TELECOMMUNICATION APPLICATIONS

In 2019, South Korea, among other countries, successfully created a commercialized mobile-phone-based 5G communication platform for the first time. Based on data from the International Telecommunications Union, a 5G network can achieve a maximum transmission speed of 20 Gbps, which is 20 times faster than that of a 4G system. Furthermore, 100,000 devices per km^2 for 4G were connected, which increased to 1 million per km^2 for 5G. When discussing such devices, we must consider each component of the platform, such as filters and low-noise amplifiers (LNA). [104], [105]. Currently, most mainstream radio frequency (RF) filters are surface acoustic wave (SAW) and BAW filters. A recent milestone in the micro-RF filter technology is illustrated in Fig. 8. Compared to SAW devices, BAW filters are recognized because of their advantages such as high operating frequency, power capacity, and high Q-factor for a steeper filter design. Additionally, as discussed earlier, the high isolation and AlN compatibility with CMOS make it a dominant device for RF communication [106], [107], [108].

MEMS-based resonators can also be integrated into systems that monitor changes in pressure, acceleration, and temperature and filter a specific frequency band for RF transceivers. Currently, SAW filters operating in low-frequency band applications are composed of lithium tantalite (LiTaO3) and lithium niobate (LiNbO3) [110], [111]. However, challenges constrain the operating frequency to around 2.5 GHz [112]. Thus, based on the literature, it is evident that AlN-based devices dominate high-band applications [113]. Additionally, with Sc doping, the piezoelectric strain coefficient d33 of the AlScN thin film can increase significantly, as discussed earlier; thus, the AlScN piezoelectric thin film shows a greater advantage for emerging FBARs [114], [115], [116], [117].

Similar to other devices discussed previously, the BAW resonator structure is composed of a piezoelectric stack, and the piezoelectric film is sandwiched between two metallic electrodes. The fundamental component of the resonators is resonance, which occurs when the generated wavelength is excited at twice the thickness of the piezoelectric layer: $f_0 = v/2d$, where f_0 and v are the resonant frequency and acoustic velocity, respectively, and d is the thickness of the piezoelectric film

Factors such as the thickness of the electrode can also affect the resonant frequency because a frequency shift can be observed, which can be used to create a passband filter. Resonators are classified based on their frequency range: flexural mode resonators are used in low-frequency applications [110], [111], contour mode resonators are used in very high-to super-high-frequency applications [113], and thin-film FBARs are used in gigahertz frequency applications [114], [115], [116], [117].

Xie and Nguyen [118] demonstrated a closed-loop oscillator; the AlN-based capacitive-piezoelectric resonator was driven by a 167.3 MHz radial-contour-mode disk, and a Q-factor of 4536 was measured. The device consists of polysilicon electrodes that do not touch the AlN, but instead hover above and below the film. This novelty allows a high Q-factor to be obtained, along with further mitigation of intrinsic losses.

Ding et al. [119] fabricated an AlN-based BAW resonator and filtered it onto a SiC substrate using a GaN HEMT-compatible process. The AlN film was grown using metal–organic chemical vapor deposition. In addition, to attenuate the size of the lateral vibration pattern, the shape of the electrode was maintained pentagonal, which could effectively prolong the path length of the Lamb wave propagation and minimize the coupling effect between the bulk wave resonance and unwanted lateral modes. Based on the design process, the resonator exhibited a FoM of 60. Chen and Rinaldi [120] developed a new class of

TABLE 5. Performance comparison of AlN-based piezoelectric MEMS energy harvesters.

Author	Material	Size	Resonant Frequency.	Power	Comments
Sharma et al. [97]	AlN	0.5 µm	114 Hz	54 nW	AlN on an SOI wafer
Dow et al. [98]	AlN	1.7 µm	186 and 572 Hz	10 and 34.78 µW	Enable higher amplitude vibrations
Jackson et al. [99]	AlN	40 mm x 6 mm	30 Hz	Average power of 1.49 and 2.81 µW	Implanted leadless pacemaker
Frach et al. [100]	$AlSc_{0.57}N$ and $AlSc_{0.43}N$	8 mm x 80 mm	600 Hz to 1.1 kHz	Tens to hundreds of µW	Reactive magnetron sputtering pr ocess.
Algieri et al. [102]	AlN	1 µm	NA	1.57 µW	Biocompatible flexible harvester ba sed using PI thin elastic layer
Gablech et al. [103]	AlN	1 µm	2480 Hz	0.25 µW	Multilayer ion beam-assisted depos ition

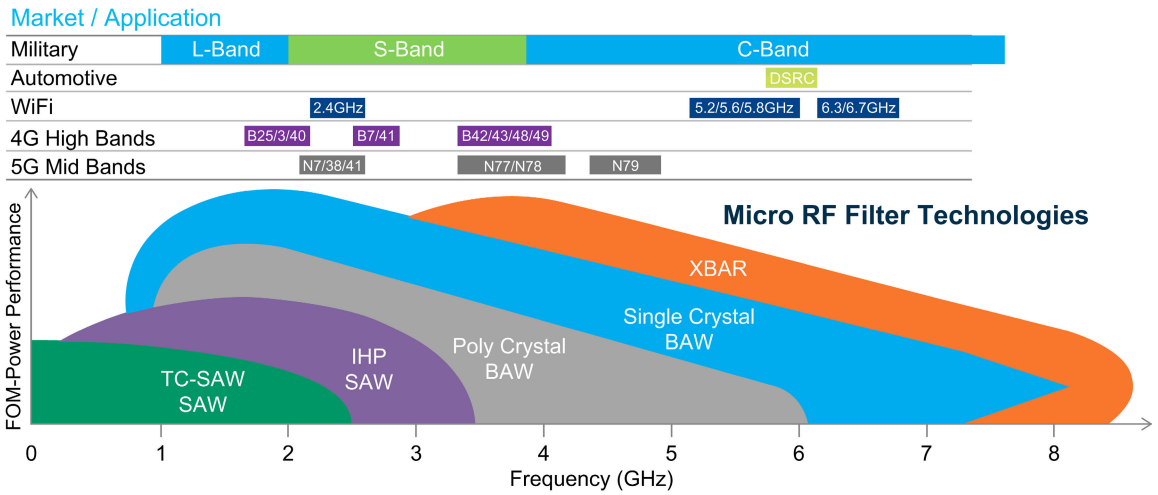

FIGURE 8. Market application and band allocation of RF filter technologies [109].

TABLE 6. Performance comparison of AlN-based telecommunication devices.

Author	Layer	Size	Resonant Frequency	Q-Factor	Notes
Xie et al. [118]	AlN	20.4	167.3 MHz	4536	The figure of Merit (FoM) of -199.1 dBc/Hz
Chen et al. [120]	AlN	1	8800 MHz	1100	A new class of overtone resonators of A2 and A3 order Asymmetrical Lamb-wave
Shahraini et al. [123]	$Al_{0.8}Sc_{0.2}N$	1	185 MHz	12.6k	Demonstration of Thickness-Lamé (TL) mode
Gao et al. [121]	AlN	1	446 MHz	1500	Bandwidth widening capability
Gao et al. [122]	AlN	1	240 MHz	3000	FoM of 52.5

overtone resonators that provided a much higher Q factor; their design utilized thicker AlN films. For overtone operation, a higher resonant frequency of up to 40 GHz is possible.

Gao et al. [121] developed an AlN Lamb wave resonator sandwiched between a series of top interdigitated transducers (IDTs) and bottom electrodes (BE). The top IDTs were alternately connected to the ground and RF signals and the BE was electrically maintained. Based on this design, the resonant frequency was set to 450 MHz. The design exhibited an electromechanical coupling of 0.94% with Q = 1500. A similar design investigated the wave reflections at anchors using time- and frequency-domain models [122]. Using both models, the authors analyzed the transient wave-anchor interaction and steady-state analysis, and evaluated the reflection coefficient. Using time-domain simulations, Lamb wave propagation was incident on the anchor. Based on this action, a stress wave and a reflected stress wave were obtained. The scattering parameter, S11, was evaluated. To increase the reflection parameter, a Pt brick layer was added to create an impedance mismatch. In comparison with the other designs mentioned by the authors, the Q-factors were found to be 3037 and 4050 based on the different thickness values of the Pt brick layer.

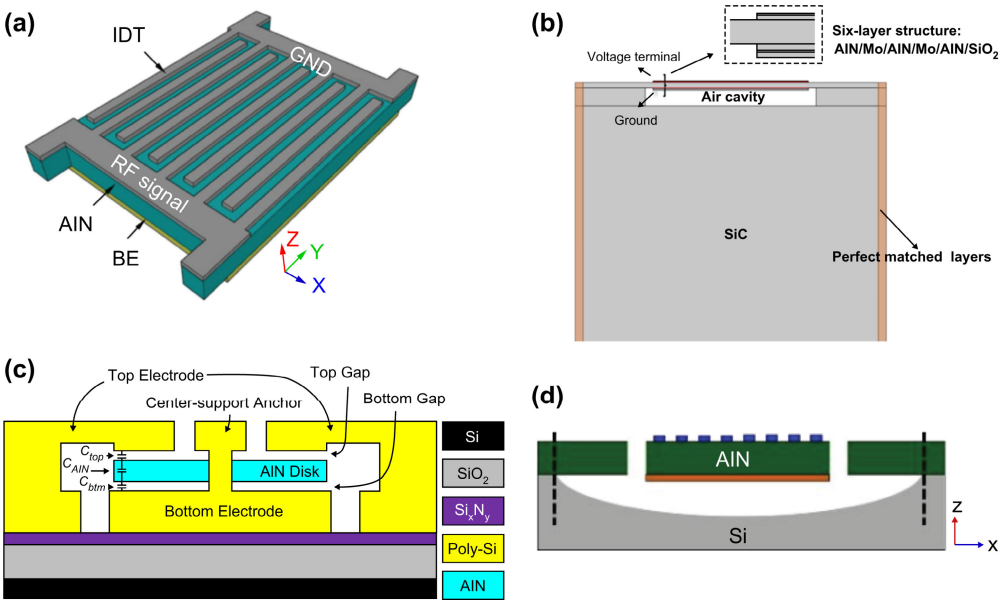

FIGURE 9. Illustration of various MEMS used in telecommunication devices: (a) prospective view and cross-sectional view of the AlN Lamb wave resonator [121], (b) model structure of the AlN BAW resonator [119], (c) cross-section view of the resonator with AlN anchored at the center [118], and (d) conventional AlN Lamb wave resonator [122].

To judge resonator performance across multiple platforms, frequency ranges, materials, and measurement configurations, researchers have used the FoM of the resonator, which is defined as FoM $=k_{eff}^2 Q$. [117]. From the literature, we can see that up to an FoM of 12.6 was achieved by Shahraini et al. [123]. The design is based on a thin-film piezoelectric substrate. The device was excited in the thickness-Lamé mode. The d31 coefficient of the device is mainly considered to excite the device in the lateral extensional modes. To excite the device in the fundamental mode, its width should be equal to the half-wavelength resonance. However, the authors used interdigitated electrode patterns to actuate the device at higher harmonics. Using interdigitated electrode patterns, the centers of the two adjacent electrodes were equal to the half-wavelength. Thus, the pure-thickness Lamé mode was actuated in the resonator.

C. INDUSTRIAL APPLICATIONS

A wide range of MEMS-based pressure sensors have been used to manage and monitor pressure-related variables in fields such as aerospace, automobile, biomedical, and oceanographic studies. Being a small footprint, more sensitive, and less expensive than its macro counterparts, it allows multiple devices to be integrated onto a single platform. The pressure sensors discussed here are based on a thin AlN layer sandwiched between a layer of metal electrodes, where AlN acts as a sensor to identify changes in pressure by producing a potential difference under the applied external stress based on the polarized c-axis because of its non centrosymmetric crystal structure [124], [125].

From the literature, we can conclude that when an AlN film is directly grown on a Si wafer, many desirable properties exist, such as a low dielectric loss tangent, efficient piezoelectric and dielectric properties, and high thermal stability [126], [127]. Kumaresan et al. [128] fabricated AlN-based ultrathin chips for pressure sensing applications. The design was based on an AlN on a Si wafer. The two proposed designs consisted of the same substrate and the same 500 nm thick AlN layer; however, a polymethylmethacrylate (PMMA) layer was spin-coated along with attaching the sensor to a flexible PI layer for the second device. The use of a PMMA layer for damage-free high-performance flexible devices ensured that the performance was not affected compared with a device without such layers.

For all microstructured devices, increasing the sensitivity of the device is critical to allowing the device to measure subtle changes. A design based on a contour-mode resonator (CMR) was experimentally verified for measurements in the 0–200 kPa pressure range. Offering enhanced linearity, the device achieved a sensitivity of 16.51 Hz/hPa [129]. Additionally, the recent use of flexible and biocompatible materials has made it possible to use smart sensors and electronic skins (e-skins) for advancements in applications such as human-machine interaction and wearable systems for health monitoring [130]. For example, Ma et al. [131] developed an ultrathin tactile sensing chip coupled with metal–oxide semiconductor field-effect transistors (MOSFETs). To achieve flexibility, the authors performed a sacrificial technique of backside lapping assisted by PMMA, which reduced stress, especially during the bonding and debonding stages. A similar use of AlN coupled with a MOSFET was reported in [132] and [133]. An industrially rated device must be employed

in harsh environments, and certain factors, such as temperature, radiation, and environmental factors, can lead to poor device performance. Therefore, changes in the interface circuit, compensation algorithms, or device modifications are required [134], [135]. Wang et al. [136] developed a solution using acoustic wave technology. The device was based on a stack of Si/AlN/Mo with IDT and Bragg-reflector-based patterns on the Mo layer. The Lamb wave pressure sensor measures absolute pressure and exhibits low-temperature drift. The resonance frequency and Q-factor were evaluated as 819.5 MHz and 10k, respectively. Xie et al. [137] proposed an oxide trench array technique to enhance the temperature stability. Using an oxide trench array, the authors presented variations in the resonance over a temperature range. To compare the effects, two devices were fabricated on the same platform: one with an oxide trench array and the other without an oxide trench array. The design with the oxide trench array exhibited minimal variation, thereby demonstrating its effectiveness.

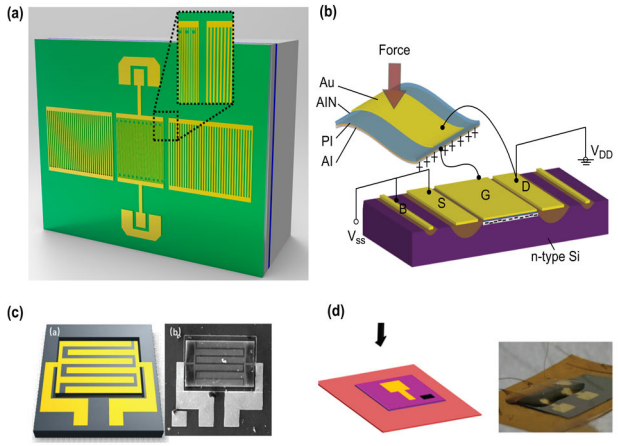

FIGURE 10. Illustration of various MEMS used as pressure sensors: (a) 3-D illustration of the acoustic wave pressure sensor [136], (b) integrated AlN capacitor with MOSFET [132], (c) schematic representative and SEM of the contour-mode resonator taken from [129], (d) optical images of the developed tactile sensor [128].

D. MEDICAL APPLICATIONS

MEMS-based pressure sensors have several advantages over their bulk counterparts. Thus, small influences on the objects can be easily detected. One such case is the accurate body readings required for medical diagnosis [139]. Furthermore, with recent developments in micromachining, high-aspect-ratio devices are now possible and devices are now able to directly measure fluctuations, variations, and anomalies in both blood pressure and blood vessels, allowing medical devices to investigate issues such as coronary heart disease and hypertension [140].

For diagnosis, continuous and noninvasive monitoring of the anatomy is critical. However, the current bulk-shaped devices are inadequate for accurate monitoring. The recent concept of stretchable electronics has achieved large-scale success, wherein a stretchable device places minimal constraints on the human body and provides continuous and noninvasive readings. Considerable efforts have been made to overcome these challenges [141], [142], [143], [144].

Recent preliminary works have reported the fabrication of similar devices based on different materials, such as 1–3 composites [145], [146]. These developments have created much hype in the medical sciences, with the idea that acoustic imaging and blood pressure monitoring can now be performed using a device that is a few inches in size. Similarly, long-term monitoring to detect anomalies has become possible owing to recent developments. Here, we compiled only the most recent developments related to the fabrication of AlN-based blood pressure measurement devices since 2015.

Bongrain et al. [147] described the design of AlN-based transducers embedded in thin, biocompatible parylene layers. The transducers were experimentally verified by measuring the fluidic pressure around the static pressure. With an excitation signal, the pressure oscillates using the flow of liquid water. Based on these variations, the sensitivity and membrane deflections were measured to determine changes in blood pressure.

A novel, self-powered sensor for arterial pulse monitoring was proposed by Dalin and Hasan [148]. The model was implemented using a self-powered sensor designed to monitor human vital signs. Based on the modeling, several analyses were performed to obtain an optimized design that included stress–strain curves, strain–applied pressure curves, and sensitivity to the elastic load.

The maximum possible nanogeneration device was achieved based on optimized geometrical features. For the verification process, various arterial pulse waveforms were used to measure the performance, and distinct peaks were detected for each case.

One limitation of the previous studies is the lack of in vitro experiments. However, an artery-diameter monitoring system using a CMOS-compatible AlN PMUT 3 $\times$ 3 mm array was suggested in [149], and an in vivo animal study was performed to demonstrate the feasibility of this system in live animals. From the experiments, the minimum diameter variation was measured as approximately 2.3 μm. However, a greater understanding of the arteries and their behavior is still needed. Pala et al. [150] studied the surface curvature of the arteries using a pulse-echo sensing method. Using simulation models of human blood vessels, the distance between the transducers and the blood vessels was maintained at 25 mm. At this distance, the time-of-flight of the echoes received from all blood vessels was the same. However, in received signals, the reflected surface curvature causes attenuation or gain, and a blood vessel with a larger diameter causes greater attenuation. For experimental verification, mineral oil inside tubes was used to imitate the acoustic property of human tissue, and by keeping the array transmitter and receiver system at a distance—to simulate the human artery position—various times-of-flight were observed.

Based on the experiment, a successful change was observed for the tubes with different diameters. Li et al. [151]

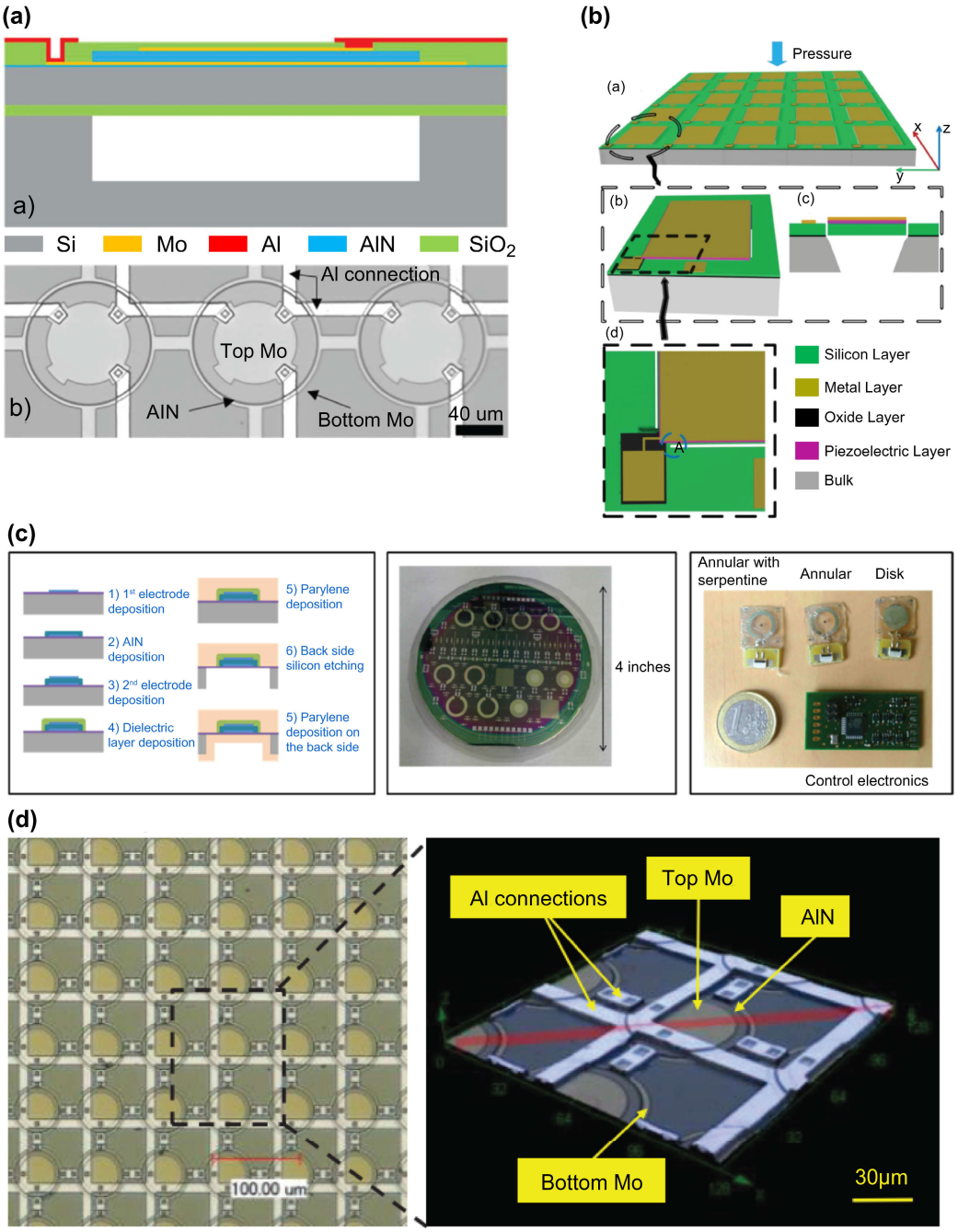

FIGURE 11. Illustration of various MEMS blood pressure monitoring devices: (a) Cross-sectional view of the PMUT array designed for in vivo monitoring [149], (b) 3D illustration of the self-powered pulse sensor array [148], (c) illustration of the fabrication process of the transducer with processed wafer and control electronics [147], (d) fabricated PMUT array with 39 × 39 elements [150].

developed a transducer and array for successful three-dimensional vascular reconstruction using both the Synthetic Aperture Focusing Technique (SAFT) and Doppler flow measurements. To verify this concept, a simulated blood vessel with two PMUTs was used. The accurate position and flow velocity were measured when the PMUTs were placed at angles of 60° in the normal direction and 30° in the horizontal direction. Two longitudinal B-mode images were obtained using the SAFT technique, and based on the placement of the devices, the accurate positions of the front and rear walls were determined. In addition, the pulse-echo method was used, and was found to be 15.101 cm/s. Chen et al. [152] grew a single-crystalline III-N film composed of AlN, AlGaN, and GaN on a Si substrate, where AlN served as a buffer layer. The sensor was designed with a thick bottom electrode to shift the neutral axis away from the piezoelectric film. The sensing mechanism relies on blood vessel expansion. When the arterial pulse travels through the vessel, it causes

TABLE 7. Performance comparison of AlN-based pressure sensors.

Author	Layer	Size	Force/Pressure Range	Sensitivity	Notes
Kumaresan et al. [128]	AlN	500 nm	NA	NA	Tactile
Ma et al. [131]	AlN	500 nm	NA	43.79 mV/N	Coupled with MOSFET chip
Gupta et al. [132]	AlN coupled MOSFET	1um	1N to 4N	2.64 V/N	Tactile
Wang et al. [136]	AlN	1 µm	0.4MPa	Q-factor of 10000	TCF of -14.4, Lamb wave based pressure sensor
Zuo et al. [129]	AlN-CMR	1.5 µm	200KPa	16.51 Hz/hPa	Monitor gaseous species
Xie at al. [137]	AlN	20 nm Seed layer and 1.2 µm as piezolayer	150 Psi	0.67% Full scale as a factor of temperature to shift in resonance	Temperature compensation with low non-linearity and thermal shift
Sujan et al. [138]	AlN	350 nm	20-bar	5 V/N	Island beam mechanism

TABLE 8. Performance comparison of AlN-based blood pressure sensors.

Author	Layer	Size	Notes
Bongrain et al. [147]	AlN	Two layers of 1000 µm and 900 nm	Use of Pt and Al as electrodes
Pala et al. [150]	AlN	3 mm × 3 mm Area and has 39 × 39 elements	k_{eff}^2 at 2.48%
Dalin et al. [148]	AlN	0.5 µm	Sensitivity of 0.13 V/kPa
Peng et al. [149]	AlN	1 µm	In vitro experiment on a sheep
Li et al. [151]	AlN	0.5 µm	Positioning of the blood vessel as well as flow velocity was tested
Chen et al. [152]	III-N with AlN as Buffer layer	0.1 µm	Detection of femoral pulse site

an increase in pressure, leading to expansion of the blood vessel. As the device is sufficiently flexible, it can bend during expansion and contraction. Based on the bending of the device, polarization was observed, which created a surface change in the device. The sensitivity of the device is an important design aspect, and the authors successfully sensed pulses at large deflection sites as well as weak pulse sites, such as the femoral artery.

IV. CONCLUSION

The recent advancements in AlN-based devices are summarized in this paper. The following key areas are focused on: the crystal structure of AlN is presented, along with a comparison of the piezoelectric properties of AlN—with 20% Sc-doped AlN and 40% Sc-doped AlN; the use of AIN in consumer-based devices, including recently developed PMUT devices, microphones, speakers, and energy harvesters is explored; furthermore, various designs of telecommunication devices, such as BAW resonators and acoustic filters for 5G applications, are presented—highlighting the importance of AlN in telecommunication devices, and the ease of fabrication as a further advantage; industrial applications of AlN-based devices—mainly pressure sensors—are presented; and finally, in the medical applications of AIN, various findings in blood pressure monitoring are presented.

From the key areas above, we can observe that PMUT device arrays as large as 110 × 56 elements have been created and have the capability to image the skin epidermis and subsurface. Similarly, for smaller arrays, the devices achieved a Q factor of up to 222 with a pressure output of 130. Similarly, for microphones, a peak sensitivity of 19 mV/Pa was achieved, and a peak SPL of up to 100 dB and a sensitivity of 105 dB/mW were observed for AlN-based speakers. Furthermore, an energy harvester with a peak power output of 854.55 $\mu W/cm^3/g^2$ have also been developed. For telecommunication devices, the Q-factor is the most important characteristic, and producing a high Q-factor in RF signals often induces nonlinear effects; however, we see that at 0.16 GHz, the devices have a Q-factor of up to 4536; similar results have been achieved in the case of pressure sensors. Finally, when we review recently developed blood pressure monitoring transducers, we investigate numerous other applications such as the imaging of internal organs [146]. AlN-based devices show potential; however, when comparing their piezo output performance, there is still room for improvement. In terms of future applications, further developments will lead to devices that can assess blood pressure waveforms and perform acoustic imaging of human organs.

AUTHOR CONTRIBUTIONS

Syed T. Haider and Muhammad A. Shah: Conceptualization and data curation, Syed T. Haider: writing—original draft, Muhammad Ali Shah: writing and analyzing of Microphone section, Duck-Gyu Lee and Shin Hur: writing—review and editing, and Shin Hur: supervision. The authors have read and agreed to the published version of this manuscript.

REFERENCES

[1] *ALN Aluminium Nitride, Sensor Technology Trend Based on AlN*. Accessed: Nov. 19, 2022. [Online]. Available: https://www.usg-platform.or.kr/comm/file/download/c8befd20-5584-4f3b-b795-aeaff560ef47

[2] M. Moreira, "Synthesis of thin piezoelectric AlN films in view of sensors and telecom applications," Ph.D. dissertation, Acta Universitatis Upsaliensis, Dept. Eng. Sci., Org. Solid State Electron., Uppsala Univ., Uppsala, Sweden, 2014.

[3] C.-H. Weng, G. Pillai, and S.-S. Li, "A thin-film piezoelectric-on-silicon MEMS oscillator for mass sensing applications," *IEEE Sensors J.*, vol. 20, no. 13, pp. 7001–7009, Jul. 2020.

[4] A. Proto, L. Rufer, S. Basrour, and M. Penhaker, "Modeling and measurement of an ultrasound power delivery system for charging implantable devices using an AlN-based pMUT as receiver," *Micromachines*, vol. 13, no. 12, p. 2127, Dec. 2022.

[5] V. Ruiz-Díez, J. Hernando-García, and J. L. Sánchez-Rojas, "Linear motors based on piezoelectric MEMS," *Multidisciplinary Digit. Publishing Inst.*, vol. 64, no. 1, p. 9, 2020.

[6] A. Khan, Z. Abas, H. S. Kim, and I.-K. Oh, "Piezoelectric thin films: An integrated review of transducers and energy harvesting," *Smart Mater. Struct.*, vol. 25, no. 5, May 2016, Art. no. 053002.

[7] V. T. Rathod, "A review of electric impedance matching techniques for piezoelectric sensors, actuators and transducers," *Electronics*, vol. 8, no. 2, p. 169, Feb. 2019.

[8] Y. Kusano, Q. Wang, G. Luo, Y. Lu, R. Q. Rudy, R. G. Polcawich, and D. A. Horsley, "Effects of DC bias tuning on air-coupled PZT piezoelectric micromachined ultrasonic transducers," *J. Microelectromech. Syst.*, vol. 27, no. 2, pp. 296–304, Apr. 2018.

[9] A. T. Le, M. Ahmadipour, and S.-Y. Pung, "A review on ZnO-based piezoelectric nanogenerators: Synthesis, characterization techniques, performance enhancement and applications," *J. Alloys Compounds*, vol. 844, Dec. 2020, Art. no. 156172.

[10] W. E. Muhea, F. M. Yigletu, R. Cabre-Rodon, and B. Iniguez, "Analytical model for Schottky barrier height and threshold voltage of AlGaN/GaN HEMTs with piezoelectric effect," *IEEE Trans. Electron Devices*, vol. 65, no. 3, pp. 901–907, Mar. 2018.

[11] S. Maouhoub, Y. Aoura, and A. Mir, "FEM simulation of AlN thin layers on diamond substrates for high frequency SAW devices," *Diamond Rel. Mater.*, vol. 62, pp. 7–13, Feb. 2016.

[12] J.-M. Wagner and F. Bechstedt, "Phonon deformation potentials of α-GaN and -AlN: An ab initio calculation," *Appl. Phys. Lett.*, vol. 77, no. 3, pp. 346–348, Jul. 2000.

[13] W. Zhou, "Thermal and dielectric properties of the AlN particles reinforced linear low-density polyethylene composites," *Thermochimica Acta*, vol. 512, nos. 1–2, pp. 183–188, Jan. 2011.

[14] S. Shelton, M.-L. Chan, H. Park, D. Horsley, B. Boser, I. Izyumin, R. Przybyla, T. Frey, M. Judy, K. Nunan, F. Sammoura, and K. Yang, "CMOS-compatible AlN piezoelectric micromachined ultrasonic transducers," in *Proc. IEEE Int. Ultrason. Symp.*, Rome, Italy, Sep. 2009, pp. 402–405.

[15] Y. Iwazaki, T. Yokoyama, T. Nishihara, and M. Ueda, "Highly enhanced piezoelectric property of co-doped AlN," *Appl. Phys. Exp.*, vol. 8, no. 6, Jun. 2015, Art. no. 061501.

[16] E. Iborra, E. Ramón, M. Clement, L. Pardo, R. López-Estopier, F. Calle, and M. Mollar, "Piezoelectric and electroacoustic properties of V-doped and Ta-doped AlN thin films," in *Proc. Joint Eur. Freq. Time Forum Int. Freq.s Control Symp. (EFTF/IFC)*, Prague, Czech Republic, Piscataway, NJ, USA, Jul. 2013, pp. 1294–1297, doi: 10.1109/EFTF-IFC.2013.6702183.

[17] S. W. Fan, K. L. Yao, Z. G. Huang, J. Zhang, G. Y. Gao, and G. H. Du, "Ti-doped AlN potential n-type ferromagnetic semiconductor: Density functional calculations," *Chem. Phys. Lett.*, vol. 482, nos. 1–3, pp. 62–65, Nov. 2009, doi: 10.1016/j.cplett.2009.09.062.

[18] Y. Kusano, G. Luo, D. Horsley, I. t. Ishii, and A. Teshigahara, "36% scandium-doped aluminum nitride piezoelectric micromachined ultrasonic transducers," in *Proc. IEEE Int. Ultrason. Symp. (IUS)*, Kobe, Japan. Piscataway, NJ, USA: IEEE, Oct. 2018, pp. 1–4, doi: 10.1109/ULTSYM.2018.8579694.

[19] D. Drury, K. Yazawa, A. Mis, K. Talley, A. Zakutayev, and G. L. Brennecka, "Understanding reproducibility of sputter-deposited metastable ferroelectric Wurtzite $Al_{0.6}Sc_{0.4}N$ films using in situ optical emission spectrometry," *Phys. Status Solidi (RRL)-Rapid Res. Lett.*, vol. 15, no. 5, May 2021, Art. no. 2100043, doi: 10.1002/pssr.202100043.

[20] Y. Liu, Y. Cai, Y. Zhang, A. Tovstopyat, S. Liu, and C. Sun, "Materials, design, and characteristics of bulk acoustic wave resonator: A review," *Micromachines*, vol. 11, no. 7, p. 630, Jun. 2020, doi: 10.3390/mi11070630.

[21] A. L. Gaeta, M. Lipson, and T. J. Kippenberg, "Photonic-chip-based frequency combs," *Nature Photon.*, vol. 13, pp. 158–169, Feb. 2019.

[22] S. Zhu, Q. Zhong, T. Hu, Y. Li, Z. Xu, Y. Dong, and N. Singh, "Aluminum nitride ultralow loss waveguides and push-pull electro-optic modulators for near infrared and visible integrated photonics," in *Proc. Opt. Fiber Commun. Conf. Exhib. (OFC)*, Mar. 2019, pp. 1–3.

[23] J. W. Stewart, J. H. Vella, W. Li, S. Fan, and M. H. Mikkelsen, "Ultrafast pyroelectric photodetection with on-chip spectral filters," *Nature Mater.*, vol. 19, no. 2, pp. 158–162, Feb. 2020.

[24] D. K. T. Ng, T. Zhang, L. Y. Siow, L. Xu, C. P. Ho, H. Cai, L. Y. T. Lee, Q. Zhang, and N. Singh, "A functional CMOS compatible MEMS pyroelectric detector using 12%-doped scandium aluminum nitride," *Appl. Phys. Lett.*, vol. 117, no. 18, Nov. 2020, Art. no. 183506.

[25] Yole DéVeloppement, "Piezoelectric devices: From bulk to thin-film 2019," Market Technol. Trends, Yole Intell., Yole Group, Lyon, France, Tech. Rep., Jun. 2019.

[26] S. E. Boeshore, *Aluminum Nitride Thin Films on Titanium: Piezoelectric Transduction on a Metal Substrate*. Ann Arbor, MI, USA: ProQuest, 2006.

[27] E. Ruiz, S. Alvarez, and P. Alemany, "Electronic structure and properties of AlN," *Phys. Rev. B, Condens. Matter*, vol. 49, no. 11, pp. 7115–7123, Mar. 1994, doi: 10.1103/PhysRevB.49.7115.

[28] V. Cimalla, J. Pezoldt, and O. Ambacher, "Group III nitride and SiC based MEMS and NEMS: Materials properties, technology and applications," *J. Phys. D, Appl. Phys.*, vol. 40, no. 20, p. 6386, 2007, doi: 10.1088/0022-3727/40/20/S16.

[29] A. Iqbal and F. Mohd-Yasin, "Reactive sputtering of aluminum nitride (002) thin films for piezoelectric applications: A review," *Sensors*, vol. 18, no. 6, p. 1797, Jun. 2018, doi: 10.3390/s18061797.

[30] G. F. Iriarte, J. G. Rodríguez, and F. Calle, "Synthesis of c-axis oriented AlN thin films on different substrates: A review," *Mater. Res. Bull.*, vol. 45, no. 9, pp. 1039–1045, Sep. 2010, doi: 10.1016/j.materresbull.2010.05.035.

[31] R. F. Dalmau, "Aluminum nitride bulk crystal growth in a resistively heated reactor," Ph.D. thesis, Dept. Mater. Sci. Eng., North Carolina State Univ., Raleigh, NC, USA, 2005. Accessed: Mar. 1, 2023. [Online]. Available: https://repository.lib.ncsu.edu/bitstream/handle/1840.16/5923/etd.pdf?sequence=1

[32] E. Kanyogoro, L. Gyugyi, and A. Mathewson, "Harnessing material defects for making latch resistors for use in mitigating linear energy transfer sensitivities in submicron CMOS SRAM cells," in *Proc. 8th Eur. Workshop Radiat. Effects Compon. Syst.*, vol. 8, 2020, p. 294.

[33] S. Barth, H. Bartzsch, D. Glöß, P. Frach, T. Modes, O. Zywitzki, G. Suchaneck, and G. Gerlach, "Magnetron sputtering of piezoelectric AlN and AlScN thin films and their use in energy harvesting applications," *Microsyst. Technol.*, vol. 22, no. 7, pp. 1613–1617, Jul. 2016.

[34] M. A. Fraga, R. F. Carvalho, G. Perin, J. P. Carmo, M. R. Meneghetti, and C. W. A. Paschoal, "Wide bandgap semiconductor thin films for piezoelectric and piezoresistive MEMS sensors applied at high temperatures: An overview," *Microsyst. Technol.*, vol. 20, pp. 9–21, Dec. 2014.

[35] T. Yanagida, Y. Fujimoto, N. Kawaguchi, and S. Yanagida, "Dosimeter properties of AlN," *J. Ceram. Soc. Jpn.*, vol. 121, no. 1420, pp. 988–991, 2013.

[36] O. Zywitzki, R. Friedlein, A. Bittner, S. Menzel, S. Schmidtmann, F. Munnik, J. Röder, G. A. Schneider, B. Wagner, and M. Wuttig, "Effect of scandium content on structure and piezoelectric properties of AlScN films deposited by reactive pulse magnetron sputtering," *Surf. Coatings Technol.*, vol. 309, pp. 417–422, Jan. 2017, doi: 10.1016/j.surfcoat.2016.11.083.

[37] G. Villanueva, "Aluminum scandium nitride as piezoelectric material for SAW/BAW hybrid resonators with large figure of merit," STI-IGM-NEMS, École Polytechn. Fédérale de Lausanne (EPFL), Lausanne, Switzerland, 2021. Accessed: Nov. 1, 2022. [Online]. Available: https://infoscience.epfl.ch/record/285661

[38] X. Jiang, H. Tang, Y. Lu, E. J. Ng, J. M. Tsai, B. E. Boser, and D. A. Horsley, "Ultrasonic fingerprint sensor with transmit beamforming based on a PMUT array bonded to CMOS circuitry," *IEEE Trans. Ultrason., Ferroelectr., Freq. Control*, vol. 64, no. 9, pp. 1401–1408, Sep. 2017, doi: 10.1109/TUFFC.2017.2703606.

[39] K. J. Son, P. Gheibi, G. Stybayeva, A. Rahimian, and A. Revzin, "Detecting cell-secreted growth factors in microfluidic devices using bead-based biosensors," *Microsyst. Nanoeng.*, vol. 3, no. 1, p. 17025, Jul. 2017, doi: 10.1038/micronano.2017.25.

[40] Y. H. Jung, S. K. Hong, H. S. Wang, J. H. Han, T. X. Pham, H. Park, J. Kim, S. Kang, C. D. Yoo, and K. J. Lee, "Flexible piezoelectric acoustic sensors and machine learning for speech processing," *Adv. Mater.*, vol. 32, no. 35, Sep. 2020, Art. no. 1904020, doi: 10.1002/adma.201904020.

[41] A. Yildirim, J. C. Grant, G. Song, S. Yook, Z. Mutlu, S. Peana, A. Dhanabal, S. K. Sinha, R. Daniels, K. M. Bellisario, G. A. Sotzing, D. H. Huston, B. C. Pijanowksi, R. Rahimi, Y. Liu, and M. Cakmak, "Roll-to-roll production of novel large-area piezoelectric films for transparent, flexible, and wearable fabric loudspeakers," *Adv. Mater. Technol.*, vol. 5, no. 7, Jul. 2020, Art. no. 2000296, doi: 10.1002/admt.202000296.

[42] I Zamora, Á. Moscoso, and J. García-Fernández, "Monolithic single PMUT-on-CMOS ultrasound system with +17 dB SNR for imaging applications," *IEEE Access*, vol. 8, pp. 142785–142794, 2020.

[43] C. Wang, X. Chen, L. Wang, M. Makihata, H.-C. Liu, T. Zhou, and X. Zhao, "Bioadhesive ultrasound for long-term continuous imaging of diverse organs," *Science*, vol. 377, no. 6605, pp. 517–523, Jul. 2022.

[44] M. Micucci and A. Iula, "Ultrasound wrist vein pattern for biometric recognition," in *Proc. IEEE Int. Ultrason. Symp. (IUS)*, Oct. 2022, pp. 1–4.

[45] C. Wang, B. Qi, M. Lin, Z. Zhang, M. Makihata, B. Liu, S. Zhou, Y.-H. Huang, H. Hu, Y. Gu, Y. Chen, Y. Lei, T. Lee, S. Chien, K.-I. Jang, E. B. Kistler, and S. Xu, "Continuous monitoring of deep-tissue haemodynamics with stretchable ultrasonic phased arrays," *Nature Biomed. Eng.*, vol. 5, no. 7, pp. 749–758, Jul. 2021.

[46] A. Iula, "Ultrasound systems for biometric recognition," *Sensors*, vol. 19, no. 10, p. 2317, May 2019.

[47] H. Nazemi, J. A. Balasingam, S. Swaminathan, K. Ambrose, M. U. Nathani, T. Ahmadi, Y. B. Lopez, and A. Emadi, "Mass sensors based on capacitive and piezoelectric micromachined ultrasonic transducers—CMUT and PMUT," *Sensors*, vol. 20, no. 7, p. 2010, Apr. 2020.

[48] Y. Qiu, J. Gigliotti, M. Wallace, F. Griggio, C. Demore, S. Cochran, and S. Trolier-McKinstry, "Piezoelectric micromachined ultrasound transducer (PMUT) arrays for integrated sensing, actuation and imaging," *Sensors*, vol. 15, no. 4, pp. 8020–8041, Apr. 2015.

[49] J. Cai, Y. Wang, D. Jiang, S. Zhang, Y. A. Gu, L. Lou, F. Gao, and T. Wu, "Beyond fundamental resonance mode: High-order multi-band ALN PMUT for in vivo photoacoustic imaging," *Microsyst. Nanoeng.*, vol. 8, no. 1, pp. 1–12, 2022, doi: 10.1038/s41378-021-00305-2.

[50] A. Ross and A. Jai, "Biometric sensor interoperability: A case study in fingerprints," in *Proc. Int. Workshop Biometric Authentication*. Berlin, Germany: Springer, 2004, pp. 134–145.

[51] R. J. Askim, M. Mahmoudi, and K. S. Suslick, "Optical sensor arrays for chemical sensing: The optoelectronic nose," *Chem. Soc. Rev.*, vol. 42, no. 22, pp. 8649–8682, 2013, doi: 10.1039/C3CS60147A.

[52] H. Kang, B. Lee, H. Kim, D. Shin, and J. Kim, "A study on performance evaluation of fingerprint sensors," in *Proc. Int. Conf. Audio-Video-Based Biometric Person Authentication*. Berlin, Germany: Springer, 2003, pp. 574–583.

[53] Y. Liao, C. Chang, C. Lin, J. You, H. Hsieh, J. Chen, A. Cho, Y. Liu, Y. Lai, J. Tseng, M. Chiang, and Y. Lin, "Flat panel fingerprint optical sensor using TFT technology," in *Proc. IEEE SENSORS*, Nov. 2015, pp. 1–4, doi: 10.1109/ICSENS.2015.7370374.

[54] X. Jiang, Y. Lu, H.-Y. Tang, J. M. Tsai, E. J. Ng, M. J. Daneman, B. E. Boser, and D. A. Horsley, "Monolithic ultrasound fingerprint sensor," *Microsyst. Nanoeng.*, vol. 3, no. 1, p. 17059, Nov. 2017, doi: 10.1038/micronano.2017.59.

[55] J. Mufioz, F. Torres, A. Uranga, V. Tsanov, N. Bamiol, E. Marigó, and M. Soundara-Pandian, "Monolithical AlN PMUT on pre-processed CMOS substrate," in *Proc. IEEE Int. Freq. Control Symp. (IFCS)*, May 2018, pp. 1–3, doi: 10.1109/FCS.2018.8597560.

[56] E. Ledesma, I. Zamora, F. Torres, A. Uranga, V. Tzanov, N. Barniol, E. Marigo, and M. Soundara-Pandian, "AlN piezoelectric micromachined ultrasonic transducer array monolithically fabricated on top of pre-processed CMOS substrates," in *Proc. 20th Int. Conf. Solid-State Sens., Actuators Microsyst. Eurosensors (TRANSDUCERS EUROSENSORS)*, Jun. 2019, pp. 655–658, doi: 10.1109/TRANSDUCERS.2019.8808706.

[57] Y. Lu, Q. Wang, and D. A. Horsley, "Piezoelectric micromachined ultrasonic transducers with increased coupling coefficient via series transduction," in *Proc. IEEE Int. Ultrason. Symp. (IUS)*, Taipei, Taiwan, Oct. 2015, pp. 1–4, doi: 10.1109/ULTSYM.2015.0093.

[58] E. Ledesma, I. Zamora, F. Torres, A. Uranga, V. Tzanov, N. Barniol, E. Marigo, and M. Soundara-Pandian, "AlN piezoelectric micromachined ultrasonic transducer array monolithically fabricated on top of pre-processed CMOS substrates," in *Proc. 20th Int. Conf. Solid-State Sens., Actuators Microsyst. Eurosensors (TRANSDUCERS EUROSENSORS)*, Jun. 2019, pp. 1669–1672.

[59] A. Uranga, G. Sobreviela, E. Marigó, M. Soundara-Pandian, and N. Barniol, "Above-IC 300 MHz AIN SAW oscillator," in *Proc. 19th Int. Conf. Solid-State Sens., Actuators Microsyst. (TRANSDUCERS)*, Kaohsiung, Taiwan. Piscataway, NJ, USA: IEEE, Jun. 2017, pp. 1927–1930.

[60] E. Ledesma, A. Uranga, F. Calle, M. Zabala, J. L. Sánchez-Rojas, J. Hernando-García, and F. J. Castaño, "Enhancing AlN PMUTs' acoustic responsivity within a MEMS-on-CMOS process," *Sensors*, vol. 21, no. 24, p. 8447, 2019.

[61] X. Jiang, H. Tang, Y. Lu, Li, Xi, J. M. Tsai, E. J. Ng, M. J. Daneman, M. Lim, F. Assaderaghi, B. E. Boser, and D. A. Horsley, "Monolithic 591×438 DPI ultrasonic fingerprint sensor," in *Proc. IEEE 29th Int. Conf. Micro Electro Mech. Syst. (MEMS)*, Shanghai, China. Piscataway, NJ, USA: IEEE, Jan. 2016, pp. 107–110.

[62] D. A. Horsley, Y. Lu, H. Tang, X. Jiang, B. E. Boser, J. M. Tsai, E. J. Ng, and M. J. Daneman, "Ultrasonic fingerprint sensor based on a PMUT array bonded to CMOS circuitry," in *Proc. IEEE Int. Ultrason. Symp. (IUS)*, Tours, France. Piscataway, NJ, USA: IEEE, Sep. 2016, pp. 1–4.

[63] W. Liu, L. He, X. Wang, J. Zhou, W. Xu, N. Smagin, M. Toubal, H. Yu, Y. Gu, J. Xu, D. Remiens, and J. Ren, "3D FEM analysis of high-frequency AlN-based PMUT arrays on cavity SOI," *Sensors*, vol. 19, no. 20, p. 4450, Oct. 2019.

[64] E. Marigó and M. Soundara-Pandian, "Frequency and acoustic performance tunability for a SiN-AlScN based PMUT device," in *Proc. Joint Conf. IEEE Int. Freq. Control Symp. Int. Symp. Appl. Ferroelectrics (IFCS-ISAF)*, Vancouver, BC, Canada. Piscataway, NJ, USA: IEEE, Jul. 2020, pp. 449–452.

[65] Q. Wang, Y. Lu, S. Mishin, Y. Oshmyansky, and D. A. Horsley, "Design, fabrication, and characterization of scandium aluminum nitride-based piezoelectric micromachined ultrasonic transducers," *J. Microelectromech. Syst.*, vol. 26, no. 5, pp. 1132–1139, Oct. 2017, doi: 10.1109/JMEMS.2017.2712101.

[66] M. Ji, H. Yang, Y. Zhou, X. Xiu, H. Lv, and S. Zhang, "Bimorph dual-electrode ScAlN PMUT with two terminal connections," *Micromachines*, vol. 13, no. 12, p. 2260, Dec. 2022, doi: 10.3390/mi13122260.

[67] E. Ledesma, I. Zamora, A. Uranga, and N. Barniol, "9.5 % scandium doped ALN PMUT compatible with pre-processed CMOS substrates," in *Proc. IEEE 34th Int. Conf. Micro Electro Mech. Syst. (MEMS)*, Jan. 2021, pp. 887–890, doi: 10.1109/MEMS51782.2021.9375359.

[68] S. Trolier-McKinstry and P. Muralt, "Thin film piezoelectrics for MEMS," *J. Electroceramics*, vol. 12, nos. 1–2, pp. 7–17, Apr. 2004, doi: 10.1023/B:JECR.0000020910.77809.b2.

[69] C.-B. Eom and S. Trolier-McKinstry, "Thin-film piezoelectric MEMS," *MRS Bull.*, vol. 37, no. 11, pp. 1007–1017, Nov. 2012, doi: 10.1557/mrs.2012.273.

[70] M. D. Williams, B. A. Griffin, T. N. Reagan, J. R. Underbrink, and M. Sheplak, "An AlN MEMS piezoelectric microphone for aeroacoustic applications," *J. Microelectromech. Syst.*, vol. 21, no. 2, pp. 270–283, Apr. 2012, doi: 10.1109/JMEMS.2011.2176921.

[71] R. J. Littrell, "High performance piezoelectric MEMS microphones," Ph.D. dissertation, Dept. Mech. Eng., Univ. Michigan, 2010.

[72] A. Rahaman, A. Ishfaque, H. Jung, and B. Kim, "Bio-inspired rectangular shaped piezoelectric MEMS directional microphone," *IEEE Sensors J.*, vol. 19, no. 1, pp. 88–96, Jan. 2019, doi: 10.1109/JSEN.2018.2873781.

[73] A. Rahaman, C. H. Park, and B. Kim, "Design and characterization of a MEMS piezoelectric acoustic sensor with the enhanced signal-to-noise ratio," *Sens. Actuators A, Phys.*, vol. 311, Aug. 2020, Art. no. 112087, doi: 10.1016/j.sna.2020.112087.

[74] P. G. Ullmann, C. Bretthauer, M. Schneider, and U. Schmid, "Stress analysis of circular membrane-type MEMS microphones with piezoelectric read-out," *Sensors*, vol. 22, Jan. 2022, Art. no. 114003, doi: 10.3390/s2202114003.

[75] R. S. Fazzio, T. Lamers, O. Buccafusca, A Goel, and W. Dauksher, "Design and performance of aluminum nitride piezoelectric microphones," in *Proc. Int. Solid-State Sens., Actuators Microsyst. Conf. (TRANSDUCERS)*, Lyon, France, Jun. 2007, pp. 1255–1258, doi: 10.1109/SENSOR.2007.4300388.

[76] E. Kim, J. Lee, S. Ahn, H. Jeon, and K. Lee, "Cell culture over nanopatterned surface fabricated by holographic lithography and nanoimprint lithography," in *Proc. 3rd IEEE Int. Conf. Nano/Micro Engineered Mol. Syst.*, Sanya, China, Jan. 2008, pp. 637–640, doi: 10.1109/NEMS.2008.4484431.

[77] Y. Zhang, R. Bauer, J. F. C. Windmill, and D. Uttamchandani, "Multi-band asymmetric piezoelectric MEMS microphone inspired by the ormia ochracea," in *Proc. IEEE 29th Int. Conf. Micro Electro Mech. Syst. (MEMS)*, Shanghai, China, Jan. 2016, pp. 1114–1117, doi: 10.1109/MEMSYS.2016.7421830.

[78] J. Segovia-Fernandez, S. Sonmezoglu, S. T. Block, Y. Kusano, J. M. Tsai, R. Amirtharajah, and D. A. Horsley, "Monolithic piezoelectric aluminum nitride MEMS-CMOS microphone," in *Proc. 19th Int. Conf. Solid-State Sens., Actuators Microsystems (TRANSDUCERS)*, Kaohsiung, Taiwan, Jun. 2017, pp. 414–417, doi: 10.1109/TRANSDUCERS.2017.7994075.

[79] A. Kumar, M. Prasad, V. Janyani, and R. P. Yadav, "Fabrication and simulation of piezoelectric aluminium nitride based micro electro mechanical system acoustic sensor," *J. Nanoelectron. Optoelectron.*, vol. 14, no. 9, pp. 1267–1274, 2019, doi: 10.1166/jno.2019.2702.

[80] H. Wang, Z. Chen, and H. Xie, "A. high-SPL piezoelectric MEMS loud speaker based on thin ceramic PZT," *Sens. Actuators A, Phys.*, vol. 20, Jul. 2020, Art. no. 112018, doi: 10.3390/s20194155.

[81] H. Wang, Y. Ma, Q. Zheng, K. Cao, Y. Lu, and H. Xie, "Review of recent development of MEMS speakers," *Micromachines*, vol. 12, no. 10, p. 1257, Oct. 2021, doi: 10.3390/mi12101257.

[82] H. Wang, P. X.-L. Feng, and H. Xie, "A dual-electrode MEMS speaker based on ceramic PZT with improved sound pressure level by phase tuning," in *Proc. IEEE 34th Int. Conf. Micro Electro Mech. Syst. (MEMS)*, Jan. 2021, pp. 701–704.

[83] K. W. Cho, S. H. Yi, Y. H. Son, and S. Y. Kweon, "Characteristics of piezoelectric micro-speaker fabricated with ZNO thin film," *Integr. Ferroelectr.*, vol. 89, no. 1, pp. 141–149, Apr. 2007.

[84] X.-H. Xu, H.-S. Wu, C.-J. Zhang, and Z.-H. Jin, "Morphological properties of AlN piezoelectric thin films deposited by DC reactive magnetron sputtering," *Thin Solid Films*, vol. 388, nos. 1–2, pp. 62–67, Jun. 2001.

[85] W. Yang, Z. Liu, D.-L. Peng, F. Zhang, H. Huang, Y. Xie, and Z. Wu, "Room-temperature deposition of transparent conducting Al-doped ZnO films by RF magnetron sputtering method," *Appl. Surf. Sci.*, vol. 255, no. 11, pp. 5669–5673, Mar. 2009.

[86] S. Yi, S. C. Ur, and E. S. Kim, "Performance of packaged piezoelectric microspeakers depending on the material properties," in *Proc. IEEE 22nd Int. Conf. Micro Electro Mech. Syst.*, Jan. 2009, pp. 765–768.

[87] A. Fawzy, Y. Lang, and M. Zhang, "Design and analysis of piezoelectric MEMS micro-speaker based on scandium-doped AlN thin film," *Micro Nano Lett.*, vol. 16, no. 3, pp. 227–231, Mar. 2021.

[88] A. Hossam and A. Fawzy, "Modeling and analysis of high-performance piezoelectric MEMS microspeaker," *Int. J.*, vol. 16, no. 1, p. 18, 2021.

[89] J. Jang, J. Lee, S. Woo, D. J. Sly, L. J. Campbell, J.-H. Cho, S. J. O'Leary, M.-H. Park, S. Han, J.-W. Choi, J. H. Jang, and H. Choi, "A microelectromechanical system artificial basilar membrane based on a piezoelectric cantilever array and its characterization using an animal model," *Sci. Rep.*, vol. 5, no. 1, pp. 1–13, Jul. 2015.

[90] C. Liu, M. Zhang, M. Sun, L. Xu, Y. Lang, S. Gong, and W. Pang, "Ultrahigh-sensitivity piezoelectric AlN MEMS speakers enabled by analytical expressions," *J. Microelectromech. Syst.*, vol. 31, no. 4, pp. 664–672, Aug. 2022.

[91] M. M. H. Shuvo, T. Titirsha, N. Amin, and S. K. Islam, "Energy harvesting in implantable and wearable medical devices for enduring precision healthcare," *Energies*, vol. 15, no. 20, p. 7495, Oct. 2022.

[92] T. He, X. Guo, and C. Lee, "Flourishing energy harvesters for future body sensor network: From single to multiple energy sources," *iScience*, vol. 24, no. 1, Jan. 2021, Art. no. 101934.

[93] L. Liu, X. Guo, W. Liu, and C. Lee, "Recent progress in the energy harvesting technology—From self-powered sensors to self-sustained IoT, and new applications," *Nanomaterials*, vol. 11, no. 11, p. 2975, Nov. 2021.

[94] C. Xu, Y. Song, M. Han, and H. Zhang, "Portable and wearable self-powered systems based on emerging energy harvesting technology," *Microsyst. Nanoeng.*, vol. 7, no. 1, pp. 1–14, Mar. 2021.

[95] Q. Jing, G. Zhu, P. Bai, Y. Xie, J. Chen, R. P. S. Han, and Z. L. Wang, "Case-encapsulated triboelectric nanogenerator for harvesting energy from reciprocating sliding motion," *ACS Nano*, vol. 8, no. 4, pp. 3836–3842, Apr. 2014.

[96] R. Yang, Y. Qin, C. Li, G. Zhu, and Z. L. Wang, "Converting biomechanical energy into electricity by a muscle-movement-driven nanogenerator," *Nano Lett.*, vol. 9, no. 3, pp. 1201–1205, Mar. 2009.

[97] A. Sharma, O. Z. Olszewski, J. Torres, A. Mathewson, and R. Houlihan, "Fabrication, simulation and characterisation of MEMS piezoelectric vibration energy harvester for low frequency," *Proc. Eng.*, vol. 120, pp. 645–650, Jan. 2015.

[98] A. B. A. Dow, A. Bittner, U. Schmid, and N. P. Kherani, "Design, fabrication and testing of a piezoelectric energy microgenerator," *Microsyst. Technol.*, vol. 20, nos. 4–5, pp. 1035–1040, Apr. 2014.

[99] N. Jackson, O. Z. Olszewski, C. O'Murchu, and A. Mathewson, "Shock-induced aluminum nitride based MEMS energy harvester to power a leadless pacemaker," *Sens. Actuators A, Phys.*, vol. 264, pp. 212–218, Sep. 2017.

[100] P. Frach, U. Schmid, T. Ferber, S. Rzepka, and J. Müller, "Energy harvesting based on piezoelectric AlN and AlScN thin films deposited by high rate sputtering," in *Proc. 9th Micro-Nanotechnol. Sensors Syst Appl.*, Anaheim, CA, USA, vol. 10194, Apr. 2017, pp. 9–13.

[101] X. He, Q. Wen, Z. Lu, Z. Shang, and Z. Wen, "A micro-electromechanical systems based vibration energy harvester with aluminum nitride piezoelectric thin film deposited by pulsed direct-current magnetron sputtering," *Appl. Energy*, vol. 228, pp. 881–890, Oct. 2018.

[102] L. Algieri, M. T. Todaro, F. Guido, V. Mastronardi, D. Desmaële, A. Qualtieri, C. Giannini, T. Sibillano, and M. De Vittorio, "Flexible piezoelectric energy-harvesting exploiting biocompatible AlN thin films grown onto spin-coated polyimide layers," *ACS Appl. Energy Mater.*, vol. 1, pp. 5203–5210, Oct. 2018.

[103] I. Gablech, J. Klempa, J. Pekárek, P. Vyroubal, J. Hrabina, M. Holá, J. Kunz, J. Brodský, and P. Neužil, "Simple and efficient AlN-based piezoelectric energy harvesters," *Micromachines*, vol. 11, no. 2, p. 143, Jan. 2020.

[104] *6G, Opens the Age of Hyper-Connection*, ETRI, Jul. 2021, vol. 179. Accessed: Jan. 15, 2023. [Online]. Available: http://www.etri.re.kr/webzine/20210709/sub01.html

[105] R. Abdolvand, B. Bahreyni, J. Lee, and F. Nabki, "Micromachined resonators: A review," *Micromachines*, vol. 7, no. 9, p. 160, Sep. 2016, doi: 10.3390/mi7090160.

[106] H. Nakamura, H. Nakanishi, T. Tsurunari, K. Matsunami, Y. Iwasaki, K.-Y. Hashimoto, and M. Yamaguchi, "Miniature surface acoustic wave duplexer using SiO_2/Al/$LiNbO_3$ structure for wide-band code-division multiple-access system," *Jpn. J. Appl. Phys.*, vol. 47, no. 5, pp. 4052–4055, May 2008.

[107] R. Mahameed, N. Sinha, M. B. Pisani, and G. Piazza, "Dual-beam actuation of piezoelectric AlN RF MEMS switches monolithically integrated with AlN contour-mode resonators," *J. Micromech. Microeng.*, vol. 18, no. 10, Oct. 2008, Art. no. 105011.

[108] T. Yokoyama, Y. Iwazaki, Y. Onda, T. Nishihara, Y. Sasajima, and M. Ueda, "Highly piezoelectric co-doped AlN thin films for wideband FBAR applications," *IEEE Trans. Ultrason., Ferroelectr., Freq. Control*, vol. 62, no. 6, pp. 1007–1015, Jun. 2015.

[109] Akoustis Technologies. *XBARTM Technology*. Accessed: May 17, 2020. [Online]. Available: https://akoustis.com/technologypresentations/xbaw-technology/

[110] K.-Y. Hashimoto, M. Kadota, T. Nakao, M. Ueda, M. Miura, H. Nakamura, H. Nakanishi, and K. Suzuki, "Recent development of temperature compensated SAW devices," in *Proc. IEEE Int. Ultrason. Symp.*, Orlando, FL, USA, Oct. 2011, pp. 79–86.

[111] H. Yunhong, Z. Meng, H. Guowei, S. Chaowei, Z. Yongmei, and N. Jin, "A review: Aluminum nitride MEMS contour-mode resonator," *J. Semicond.*, vol. 37, no. 10, 2016, Art. no. 101001, doi: 10.1088/1674-4926/37/10/101001.

[112] G. Piazza, P. J. Stephanou, and A. P. Pisano, "Piezoelectric aluminum nitride vibrating contour-mode MEMS resonators," *J. Microelectromech. Syst.*, vol. 15, no. 6, pp. 1406–1418, Dec. 2006, doi: 10.1109/JMEMS.2006.886612.

[113] G. Pillai, A. A. Zope, J. M. Tsai, and S. Li, "Design and optimization of SHF composite FBAR resonators," *IEEE Trans. Ultrason., Ferroelectr., Freq. Control*, vol. 64, no. 12, pp. 1864–1873, Dec. 2017, doi: 10.1109/TUFFC.2017.2759811.

[114] R. Ruby, P. Bradley, J. Larson, Y. Oshmyansky, and D. Figueredo, "Ultra-miniature high-Q filters and duplexers using FBAR technology," in *IEEE Int. Solid-State Circuits Conf. (ISSCC) Dig. Tech. Papers*, San Francisco, CA, USA, Feb. 2001, pp. 120–121, doi: 10.1109/ISSCC.2001.912303.

[115] C. Nguyen, "MEMS technology for timing and frequency control," *IEEE Trans. Ultrason., Ferroelectr. Freq. Control*, vol. 54, no. 2, pp. 251–270, Feb. 2007, doi: 10.1109/TUFFC.2007.240.

[116] R. Ruby, "Review and comparison of bulk acoustic wave FBAR, SMR technology," in *Proc. IEEE Ultrason. Symp.*, New York, NY, USA, Oct. 2007, pp. 1029–1040, doi: 10.1109/ULTSYM.2007.266.

[117] G. Pillai, A. A. Zope, J. M.-L. Tsai, and S.-S. Li, "Piezoelectric MEMS resonators: A review," *IEEE Sensors J.*, vol. 21, no. 11, pp. 12589–12605, Jun. 2021, doi: 10.1109/JSEN.2021.3073505.

[118] Q. Xie and C. T.-C. Nguyen, "167-MHz AlN capacitive-piezoelectric oscillator," in *Proc. IEEE Int. Ultrason. Symp. (IUS)*, Las Vegas, NV, USA, Sep. 2020, pp. 1–4, doi: 10.1109/IUS46767.2020.9251799.

[119] R. Ding, W. Xuan, S. Dong, B. Zhang, F. Gao, G. Liu, Z. Zhang, H. Jin, and J. Luo, "The 3.4 GHz BAW RF filter based on single crystal AlN resonator for 5G application," *Nanomaterials*, vol. 12, no. 17, p. 3082, Sep. 2022, doi: 10.3390/nano12173082.

[120] G. Chen and M. Rinaldi, "High-Q X band aluminum nitride combined overtone resonators," in *Proc. Joint Conf. IEEE Int. Freq. Control Symp. Eur. Freq. Time Forum (EFTF/IFC)*, Orlando, FL, USA, Apr. 2019, pp. 1–3, doi: 10.1109/FCS.2019.8856047.

[121] A. Gao, K. Liu, J. Liang, and T. Wu, "AlN MEMS filters with extremely high bandwidth widening capability," *Microsyst. Nanoeng.*, vol. 6, no. 1, pp. 1–11, Sep. 2020.

[122] A. Gao, M. Winterkorn, Y. Yang, R. Lu, J. Provine, and S. Gong, "Boosting Qs of AlN resonators by redefining acoustic boundaries," in *Proc. IEEE 32nd Int. Conf. Micro Electro Mech. Syst. (MEMS)*, Jan. 2019, pp. 883–886.

[123] S. Shahraini, H. Mansoorzare, A. Mahigir, and R. Abdolvand, "Thickness-Lamé thin-film piezoelectric-on-silicon resonators," *J. Microelectromech. Syst.*, vol. 29, no. 3, pp. 296–305, Jun. 2020.

[124] S. Jena and A. Gupta, "Review on pressure sensors: A perspective from mechanical to micro-electro-mechanical systems," *Sensor Rev.*, vol. 41, no. 3, pp. 320–329, Aug. 2021.

[125] R. B. Mishra, N. El-Atab, A. M. Hussain, and M. M. Hussain, "Recent progress on flexible capacitive pressure sensors: From design and materials to applications," *Adv. Mater. Technol.*, vol. 6, no. 4, Apr. 2021, Art. no. 2001023.

[126] N. Yogeswaran, E. S. Hosseini, and R. Dahiya, "Graphene based low voltage field effect transistor coupled with biodegradable piezoelectric material based dynamic pressure sensor," *ACS Appl. Mater. Interfaces*, vol. 12, no. 48, pp. 54035–54040, Dec. 2020.

[127] S. Gupta, N. Yogeswaran, F. Giacomozzi, L. Lorenzelli, and R. Dahiya, "Touch sensor based on flexible AlN piezocapacitor coupled with MOSFET," *IEEE Sensors J.*, vol. 20, no. 13, pp. 6810–6817, Jul. 2020.

[128] Y. Kumaresan, S. Ma, D. Shakthivel, and R. Dahiya, "AlN ultra-thin chips based flexible piezoelectric tactile sensors," in *Proc. IEEE Int. Conf. Flexible Printable Sensors Syst. (FLEPS)*, Jun. 2021, pp. 1–4.

[129] J. Zuo, H. Zhang, Y. Chang, J. Liang, W. Pang, and X. Duan, "Highly sensitive AlN contour-mode resonator-based pressure sensor for in-line monitoring of chemical reactions," in *Proc. 20th Int. Conf. Solid-State Sens., Actuators Microsystems Eurosensors (TRANSDUCERS EUROSENSORS)*, Jun. 2019, pp. 1373–1376.

[130] L. Wang, K. Jiang, and G. Shen, "Wearable, implantable, and interventional medical devices based on smart electronic skins," *Adv. Mater. Technol.*, vol. 6, no. 6, Jun. 2021, Art. no. 2100107.

[131] S. Ma, Y. Kumaresan, A. S. Dahiya, L. Lorenzelli, and R. Dahiya, "Flexible tactile sensors using AlN and MOSFETs based ultra-thin chips," *IEEE Sensors J.*, vol. 22, no. 3, 2022, pp. 1034-1041

[132] S. Gupta, N. Yogeswaran, F. Giacomozzi, L. Lorenzelli, and R. Dahiya, "Flexible AlN coupled MOSFET device for touch sensing," in *Proc. IEEE SENSORS*, Oct. 2018, pp. 1–4.

[133] R. Takei, H. Okada, D. Noda, R. Ohta, T. Takeshita, T. Itoh, and T. Kobayashi, "High-efficiency MOSFET bridge rectifier for AlN MEMS cantilever vibration energy harvester," *Jpn. J. Appl. Phys.*, vol. 56, no. 4S, Apr. 2017, Art. no. 04CC03.

[134] Y. Javed, M. M. Mansoor, and A. S. Irtiza, "A review of principles of MEMS pressure sensing with its aerospace applications," *Sensor Rev.*, vol. 39, no. 1, pp. 38–49, 2019.

[135] P. Verma, D. Punetha, and S. K. Pandey, "Sensitivity optimization of MEMS based piezoresistive pressure sensor for harsh environment," *Silicon*, vol. 12, no. 11, pp. 2663–2671, Nov. 2020.

[136] T. Wang, Z. Tang, H. Lin, K. Zhan, J. Wan, S. Wu, Y. Gu, W. Luo, and W. Zhang, "A low temperature drifting acoustic wave pressure sensor with an integrated vacuum cavity for absolute pressure sensing," *Sensors*, vol. 20, no. 6, p. 1788, Mar. 2020.

[137] Q. Xie, N. Wang, C. Sun, A. B. Randles, P. Singh, X. Zhang, and Y. Gu, "Effectiveness of oxide trench array as a passive temperature compensation structure in AlN-on-silicon micromechanical resonators," *Appl. Phys. Lett.*, vol. 110, no. 8, Feb. 2017, Art. no. 083501.

[138] S. Yenuganti, U. Gandhi, and U. Mangalanathan, "Piezoelectric microresonant pressure sensor using aluminum nitride," *J. Micro/Nanolithogr., MEMS, MOEMS*, vol. 16, no. 2, Apr. 2017, Art. no. 025001.

[139] J. Sola, M. Proenca, D. Ferrario, J.-A. Porchet, A. Falhi, O. Grossenbacher, Y. Allemann, S. F. Rimoldi, and C. Sartori, "Noninvasive and nonocclusive blood pressure estimation via a chest sensor," *IEEE Trans. Biomed. Eng.*, vol. 60, no. 12, pp. 3505–3513, Dec. 2013.

[140] P. Song, Z. Ma, J. Ma, L. Yang, J. Wei, Y. Zhao, M. Zhang, F. Yang, and X. Wang, "Recent progress of miniature MEMS pressure sensors," *Micromachines*, vol. 11, no. 1, p. 56, Jan. 2020.

[141] T. Someya, Z. Bao, and G. G. Malliaras, "The rise of plastic bioelectronics," *Nature*, vol. 540, no. 7633, pp. 379–385, Dec. 2016.

[142] J. A. Rogers, T. Someya, and Y. Huang, "Materials and mechanics for stretchable electronics," *Science*, vol. 327, no. 5973, pp. 1603–1607, Mar. 2010.

[143] K. Meng, J. Chen, X. Li, Y. Wu, W. Fan, Z. Zhou, Q. He, X. Wang, X. Fan, Y. Zhang, J. Yang, and Z. L. Wang, "Flexible weaving constructed self-powered pressure sensor enabling continuous diagnosis of cardiovascular disease and measurement of cuffless blood pressure," *Adv. Funct. Mater.*, vol. 29, Dec. 2018, Art. no. 1806388.

[144] C. Peng, L. Zheng, Y. Yang, L. Xie, J. Wu, Z. Wu, Y. Liu, and F. Yan, "Noninvasive and nonocclusive blood pressure monitoring via a flexible piezo-composite ultrasonic sensor," *IEEE Sensors J.*, vol. 21, no. 3, pp. 2642–2650, Feb. 2021.

[145] C. Wang, Y. Li, M. Zhao, Z. Chen, X. Li, J. Zou, J. Chen, J. Jiang, J, Y. Dai, X. Liu, and P. Huang, "Bioadhesive ultrasound for long-term continuous imaging of diverse organs," *Science*, vol. 377, pp. 517–523, Jul. 2022, doi: 10.1126/science.abm3771.

[146] C. Peng, M. Chen, H. K. Sim, Y. Zhu, and X. Jiang, "A flexible piezo-composite ultrasound blood pressure sensor with silver nanowire-based stretchable electrodes," in *Proc. IEEE 15th Int. Conf. Nano/Micro Engineered Mol. Syst. (NEMS)*, Sep. 2020, pp. 143–146.

[147] A. Bongrain, L. Rousseau, L. Valbin, N. Madaoui, G. Lissorgues, F. Verjus, and P. A. Chapon, "A new technology of ultrathin AlN piezoelectric sensor for pulse wave measurement," *Proc. Eng.*, vol. 120, pp. 459–463, Jan. 2015, doi: 10.1016/j.proeng.2015.08.668.

[148] E. M. Dalin and S. M. R. Hasan, "Modeling of a novel AlN nanogenerator-based self-powered MEMS arterial-pulse sensor," *IEEE Sensors J.*, vol. 22, no. 9, pp. 8574–8582, May 2022, doi: 10.1109/JSEN.2022.3161026.

[149] Y. Peng, S. Pala, Z. Shao, H. Ding, J. Xie, and L. Lin, "Subcutaneous and continuous blood pressure monitoring by PMUTs in an ambulatory sheep," in *Proc. IEEE 35th Int. Conf. Micro Electro Mech. Syst. Conf. (MEMS)*, Kyoto, Japan, Jan. 2022, pp. 416–419, doi: 10.1109/MEMS51670.2022.9699550.

[150] S. Pala, Y. Peng, H. Ding, J. Xie, and L. Lin, "Attenuation of curved structural surfaces in PMUT measurements," in *Proc. 21st Int. Conf. Solid-State Sens., Actuators Microsyst. (TRANSDUCERS)*, Seoul, South Korea, Jun. 2021, pp. 246–249, doi: 10.1109/Transducers50396.2021.9495640.

[151] J. Li, L. Zhang, C. Yu, B. Yu, P. Niu, and Z. Wang, "Three-dimensional vascular reconstruction and Doppler flow measurement using PMUTs," in *Proc. IEEE Int. Ultrason. Symp. (IUS)*, Long Beach, CA, USA, Oct. 2022, pp. 1–4, doi: 10.1109/IUS54386.2022.9957146.

[152] J. Chen, H. Liu, W. Wang, N. Nabulsi, W. Zhao, J. Y. Kim, M. Kwon, and J. Ryou, "High durable, biocompatible, and flexible piezoelectric pulse sensor using single-crystalline III-N thin film," *Adv. Funct. Mater.*, vol. 29, no. 37, Sep. 2019, Art. no. 1903162.